Assessing Chemosensitivity in 3D Breast Cancer Spheroids using Optical Coherence Tomography

By
Ramisa Fariha
B.Sc. The Pennsylvania State University 2017

Thesis

Submitted in partial fulfillment of the requirements for the
Degree of Master of Science in Biomedical Engineering at Brown University

PROVIDENCE, RHODE ISLAND

MAY 2020

Signature Page

This thesis by Ramisa Fariha is accepted in its present form by the Center of Biomedical Engineering as satisfying the thesis requirements of the degree of Master of Science.

Date: __5/1/2020_____ _____

Jonghwan Lee, Advisor

Recommended to the Graduate Council

Date: _April 30, 2020__ _____

Jeffrey Morgan, Reader

Date: 5/1/30 _____

Celinda Kofron, Reader

Approved by the Graduate Council

Date: _____ _____

Andrew G. Campbell, Dean of the Graduate School

Curriculum Vitae

Ramisa Fariha
ramisa_fariha@brown.edu

Education

Master of Science, Brown University, Providence, RI May 2020
Biomedical Engineering Cumulative GPA: 4.00/4.00
Advisor: Jonghwan Lee, Ph.D.
Thesis: *Assessing Chemosensitivity in 3D Breast Cancer Spheroids using Optical Coherence Tomography*

Bachelor of Science, The Pennsylvania State University, State College, PA. May 2017
Biomedical Engineering Cumulative GPA: 3.34/4.00

Research Experience

Graduate Student Researcher, *Lee Lab and Morgan Lab* July 2018- May 2020
Brown University Center for Biomedical Engineering

- Culturing MCF7 breast cancer tissues in 3D scaffold-free platform and conducting an anti-cancer drug study; performing method validation using Live/Dead assay.
- Imaging 3D tissues using Optical Coherence Tomography (OCT), collecting data and performing data analysis using MATLAB.

Undergraduate Research Assistant*, Lian Lab* August 2015- May 2017
The Pennsylvania State University, Department of Biomedical Engineering

- Developed chemical media for boosting hESCs and iPSCs growth and differentiation; analyzed the impact of various chemical substitutions so as to aid cell differentiation into different cell types.
- Conducted experiments with H9 hESCs to obtain better understanding of the cell lineages formed in the early embryogenesis of mesodermal layers, via collection of samples over 24-hour period; learned the growth and development of embryonic stem cells during various stages of cell differentiation (via RNA-Sequencing).

Work Experience

Research and Development Intern, *ACell Inc.* May 2017-April 2018
Urinary bladder matrix (UBM) Characterization Study

- Decellularized porcine bladders according to standard operation procedures; conducting histology via H&E staining methods; lyophilized the bladders and evaluated DNA, RNA and protein levels (BCA).
- Investigated the effect of UBM on macrophage activation in vitro: isolated macrophages from mice bone marrow and maintained cell culture; activated

macrophages with cytokines and UBM products, harvested and fixed cells; isolated RNA and synthesized cDNA for downstream qPCR assay; performed qPCR and gene expression analysis; fluorescent immunolabeled and imaged fixed cells.

Degradation Study

- Investigated the rate of degradation of varying wound sheet products using enzymatic digestion model.

DNA Specification Test

- Performed test method validation for DNA quantification, and troubleshot the assay by altering different relevant parameters.

Animal Study- Wound Study

- Investigated different wound treatments in pig models, via gene expression analysis.

Pericardial Patch Study

- Investigated Urinary Bladder Matrix (UBM) decellularization to create pericardial patch devices.

Competitor Product Study

- Compared collagen, porcine bladder and human tissue-based products by investigating the presence of various cellular components using different assays.

Publications and Poster Presentations

- **Ramisa Fariha**, Blanche Ip, Jeffrey Morgan, Jonghwan Lee. *Assessing Chemosensitivity in 3D Breast Cancer Spheroids using Optical Coherence Tomography*. (Abstract submitted for a poster presentation for Northeast Bioenegineering Conference (NEBEC), 2020).

- **Ramisa Fariha**, Blanche Ip, Jeffrey Morgan and Jonghwan Lee. *Establishing Optical Coherence Tomography (OCT) as an Effective Method for Investigating Cellular Viability in 3D Breast Cancer Spheroids.* (Poster presented at the Women in STEM Symposium (WiSTEM), 2019).

- Elie Zakhem, Luai Huleihel, Husni Alasadi, **Ramisa Fariha**, Alexander LeBrun, Hannah B Baker, Nathaniel T Remlinger, and Thomas W Gilbert. *A Comparison of the Composition and In Vitro Macrophage Response between MicroMatrix® and AmnioFill®.* (Poster presented at the Symposium of Advanced Wound Care (SAWC), November 2018.)

- Luai Huleihel, **Ramisa Fariha**, Alex LeBrun, Nathaniel T Remlinger, and Thomas W Gilbert. *The Effects of Processing on Urinary Bladder Matrix (UBM) Characteristics.* (Abstract for 10th Symposium on Biologic Scaffolds for Regenerative Medicine, May 2018).

- Lin, L., **Fariha, R**., Randolph, L., Lian, X. *Chemically Defined LaSR Medium Supports Long-term Cultivation of Human Pluripotent Stem Cells and*

Embryonic Stem Cells. (Manuscript in review)

- Witmer, E., Lin, L., **Fariha, R**., Lian, X. *RNA-Sequencing Analysis of Early Mesodermal Differentiation.* (Manuscript in review)

Teaching and Mentorship

Instructor, *Introduction to Engineering & Design* July 2019- August 2019
Summer @Brown, School of Professional Studies Providence, RI

- Designed an introductory engineering design course for high school students, to provide an understanding of the fundamentals of engineering and design processes.
- Helped students identify engineering problems, giving them an opportunity to solve them by means of designing look-like prototypes and presenting their design to the class.

Mentor and Member, *Society of Women Engineers (SWE)* August 2015-May 2017
The Pennsylvania State University State College, PA

- Mentored students at lower class standing, and from satellite campuses, explore engineering majors, especially Biomedical Engineering.
- Guided and supported engineering students through research, graduate school and job searches, as an alumna.

Selected Honors and Awards

Brown Graduate Community Fellowship 2018, 2019, 2020

- A fellowship from The Graduate Student awarded to selected students, to cultivate community as well as leadership, collaboration, and problem-solving skills through developing and implementing initiatives that strengthen the Brown graduate community.

Penn State Outstanding First Year Student of the Year 2013-2014

- An award recognizing an outstanding first-year student for character, scholarship, leadership, citizenship. This the highest rank of award an undergraduate freshman student can receive.

Dean's List, The Pennsylvania State University Fall 2013, 2016; Spring 2014

Chancellor's Scholarship, The Pennsylvania State University Fall 2014-Spring 2015

Penn State Behrend Honor's Award 2013-2015

Penn State Council of Fellows Leadership Scholarship Fall 2014-Spring 2015

Robert C. Fritz Award, Penn State College of Engineering Fall 2015

Robert and Louise Dickinson Scholarship in Engineering Fall 2015, Spring 2017

- An award by Penn State's College of Engineering, recognizing junior and senior engineering students with outstanding academic achievements.

Penn State 'Miss Blue and White' **Spring 2015**

Selected Leadership

- *Member*, Brown International Student Advisory Board
- *Assistant for Graduate School*, Brown International Graduate Orientation
- *President*, the Muslim Student Association, Penn State
- *Residence Life Service Leader*, Center for Service, Penn State
- *Co-founder*, The Dialogue, an online cultural magazine
- *Staff Writer*, Behrend Beacon
- *Welcome Week Leader*, Penn State
- *Event Staff*, the Lion Entertainment Board, Penn State
- *Member*, Lambda Sigma National Honor Society
- *Writer and Photographer*, La Vie, the Penn State Yearbook
- *Member*, Alpha Epsilon Delta, National Honor Society
- *Member*, Omicron Delta Kappa, National Leadership Honor Society

Skills

- Microtissues™ 3D tissue culture
- Optical Coherence Tomography (OCT) Imaging
- Cell Immunolabeling (Macrophages, and Live/Dead®)
- COMSOL Multiphysics
- MATLAB
- BMDM Isolation
- Mimics
- 3matic
- Fluent in Bengali
- Fluent in Hindi
- Conversational in French
- DNA Quantification (Picogreen dsDNA assay)
- Histology (H&E staining)
- RT-qPCR (Taqman Chemistry)
- RNA Isolation
- cDNA Synthesis
- RNA Quantification
- BCA Protein Assay

Other Work Experiences

Graduate Coordinator September 2019-May 2020
Global Brown Center for International Students Providence, RI

- Planned, organized and executed events for graduate international students at Brown University.

Communications Intern September 2018-March 2020
Brown Center for Biomedical Engineering Providence, RI

- Conducted interviews, attended seminars and created news content for the CBME website.

Research Assistant and Junior Copywriter Summers 2012-2015
The Kaharba Productions Dhaka, Bangladesh

- Conducted pre-production research- including project analysis, feasibility, cost of production, site inspection etc. for documentary projects for clients such as UNICEF, US Embassy, SwissContact.
- Developed web content, maintained pre and post-production paperwork, blogged for the official website and conducted social media publicity.

Student Assistant January 2014-May 2015
Admissions, Penn State, Erie Erie, PA

- Maintained international student database, served as an office assistant and worked at various events like Open house, Science fairs etc.

Acknowledgments

First of all, I would like to thank almighty Allah for all His blessings that He has bestowed upon me throughout my lifetime. I would like to thank my father Ahsanul Karim Chowdhury for always working hard, even in your seventies, to provide for my education, and for empowering me as a daughter throughout my life. I would also like to thank my mother Laila Nahar Chowdhury, for all the sacrifices you have made for me and my rights as a female child. A very special thank you to my brother Sajjadadul Karim Chowdhury- for treating me with all your love and respect, and my sister in-law, Musrat Sharmin Masri- for always cheering me on. I would like to send my special thanks to my uncles Ekramul Karim Chowdhury and Anwar Hossain, for supporting my family- financially and emotionally- during the course of my education in the United States. Thank you Towfick, Jitendra and Rajendra bhaiyas for treating me like a sibling and helping me navigate through all the difficult situations in life. I would like to convey my sincerest gratitude to my Godparents Shahjada Miah and Mehrunnesa for your unconditional love and encouragement. And a very special shout out to my nephew Vivan for always inspiring me through your drawings and for asking me all the scientific questions in the world.

I would like to convey my sincere thanks to all my teachers and mentors throughout my lifetime, especially to those at Brown University, who have helped me bring my thesis to fruition. Thanks to Dr. Jonghwan Lee for all your hard work to keep our lab functional, and for entrusting me with a project that incorporated my passion and vision. Jonghwan,

you have provided me with immense support and encouragement as a mentor during my time at Brown, for which I will always remain thankful. Thanks to Dr. Jeffrey Morgan, for being the true inspiration behind my journey to Biomedical Engineering, and for allowing me to be trained in your lab, and for all your advice and encouragement. A very special thanks to Dr. Blanche Ip for being one of the best teachers I have ever had, and for taking me under your wings and training me to be a dedicated and hardworking scientist. I would also like to thank Dr. Celinda Kofron and Dr. Marissa Gray for your constant support and guidance during my time at Brown, for helping me find my niche within Biomedical engineering, and for always going above and beyond your call of duty in order to accommodate me during my time of crisis. Thanks to Ahbid Zein-Sabatto (Lee lab) for providing me with your honest feedback and helping me troubleshoot my experiments. Thanks to Benjamin Wilks (Morgan lab) for being an incredible mentor, who has had a huge impact in my graduate student life- as a scientist and as a member of the graduate student community. Ben, you have not only provided me with guidance and advice in regard to my experiments but have also helped me become a better human being and mentor to future scientists by setting a great benchmark. Thank you to my lab mate and fellow woman in STEM, Caitlin Hopkins (Morgan lab) for all your scientific input, advice and constant support that have helped me carry out all the experiments successfully. My sincerest thanks to my fellow lab mate (Lee lab), master's cohort member and best friend Julian Montagut, for your significant scientific contribution to my research, as well as for providing me with emotional support throughout the late-night experiments and challenges during my time at Brown. A special thanks goes to Meghan Dempsey (Darling lab) for being such a wonderful lab neighbor and helping me with

occasional logistics whenever my experiments needed last minute modifications. Thank you all for the contributions you have made, and the impact you have had in my life that has allowed me to emerge as a better scientist and human being.

I will forever be indebted to the entire Global Brown community, especially OISSS and the Global Brown Center for International Students for providing me with a family here at Brown, that has helped me sustain through the challenges of Graduate School. A big thank you to Albert Soto (Counseling and Psychological Services), Jonathan Corey (Students and Employees Accessibility Services), Dean Shayna Kessel (Graduate School) and Dean Maria Suarez (Graduate School) for being the source of constant support and love to students with special needs, such as myself. Brown is lucky to have helpful members like you, who are always putting students' needs above all.

To all my best friends, here at Brown and around the world (Nasheen, Tamim, Hridoy, Mary Ellen, Kevin, Brenna, Laser, Odessa, Timo, Patrick, May, Emily, Amanda, Mary, Shuai, Pablo): thank you for being my cheerleaders, unsung heroes, entertainers and unpaid therapists. Being a scientist would not have been possible without you all.

And last but certainly not the least, I would like to thank the person who has been my gravity since 2005, my biggest inspiration behind becoming a scientist, a fellow dream chaser, and as of today, the person who has empowered me with the strength to finish this thesis simply through his words- Dave Bautista. Being the first Ivy League graduate from my hometown would not have been possible if Dave had not inspired me to dream big

and follow my dreams. Thank you, Dave, for hearing me talk about my experimental design, asking insightful questions and for always telling me how proud you are of me. You have made more scientific contributions to this study than you can comprehend. You inspire me to make science accessible to everyone, enabling me to simplify complex ideas and think outside the box. I am incredibly blessed to have you in my life.

Table of Contents

SIGNATURE PAGE ..... **II**

CURRICULUM VITAE ..... **III**

ACKNOWLEDGMENTS ..... **VIII**

LIST OF ILLUSTRATIONS ..... **XIII**

ABSTRACT ..... ERROR! BOOKMARK NOT DEFINED.

CHAPTER 1 ..... **1**

1. BACKGROUND 1
   - *1.1 Breast Cancer Research and MCF7 Cells* *1*
   - *1.2 Three-Dimensional Tissue Research: Microtissues™* *2*
   - *1.3 Chemosensitivity and Cell Viability in 3D culture tissues* *4*
   - *1.4 OCT as a Label-Free and Longitudinal Imaging Platform* *6*
   - *1.5 Choice of Drug: Paclitaxel* *7*

CHAPTER 2 ..... **8**

2. SPHEROID SEEDING DENSITY OPTIMIZATION 8
   - *2.1 Methods and Materials* *9*
   - *2.1.1 MCF7 Cell Culture* *9*
   - *2.1.2 Microtissues™: Micromold Preparation* *11*
   - *2.1.3 Microtissues Cell Seeding and Tissue Formation* *12*
   - *2.1.4 Tissue Imaging (Seeding Density)* *14*
   - *2.1.5 Data Reconstruction and Analysis* *15*
   - *2.2 Results and Discussion* *18*

CHAPTER 3 ..... **20**

3. MCF7 PROLIFERATION *IN VITRO* 20
   - *3.1 Methods and Materials* *21*
   - *3.1.1 Cell Culture and Tissue Formation* *21*
   - *3.1.2 Longitudinal in vitro Imaging* *21*
   - *3.1.3 Data Analysis: FIJI* *22*
   - *3.2 Results and Discussion* *23*

CHAPTER 4 ..... **25**

4. DOSE-TIME-RESPONSE STUDY USING PACLITAXEL: PILOT 25
   - *4.1 Method and Materials* *26*
   - *4.1.1 Cell Culture, Drug Treatment and OCT Imaging* *26*
   - *4.1.2 Live/Dead® Viability Assay* *27*
   - *4.2 Results and Discussion* *28*

CHAPTER 5 ..... **34**

5. DOSE-TIME-RESPONSE STUDY USING PACLITAXEL 34
   - *5.1 Methods and Materials* *35*
   - *5.1.1 Cell Culture, Spheroid Formation and Drug Treatment* *35*
   - *5.1.2 Live/Dead® Viability Assay and Imaging* *36*
   - *5.1.3 Longitudinal OCT Imaging using a Mini-Incubator* *39*
   - *5.1.4 Data Reconstruction, Segmentation, and Analysis* *40*
   - *5.2 Results and Discussion* *46*
   - *5.2.1 Geometry* *46*
   - *5.2.2 Intensity and Decorrelation* *50*
   - *5.2.3 Live/Dead Results* *57*

CHAPTER 6 ..... **59**

6. Conclusion and Future Direction 59
6.1 Conclusion *59*
6.2 Further Experiments and Analysis *60*
SUPPLEMENTAL FIGURES **63**
BIBLIOGRAPHY **70**

List of Illustrations

Figure 1. Breast cancer progression. 2
Figure 2. 2D versus 3D cell culture 3
Figure 3. 3D spheroid microenvironment 5
Figure 4. Schematic of OCT 7
Figure 5. A T75 cell culture flask. 9
Figure 6. A. cell pellet and cell supernatant; B. A brightfield microscope with a hemocytometer on stage,. 10
Figure 7. A 24-96 3D Petri Dish 11
Figure 8. The process of casting a gel-mold using a 3D petri dish 12
Figure 9. The process of cell self-assembly in Microtissues:. 13
Figure 10. The OCT system set up for a top-down imaging, ... 14
Figure 11. A microtissue focused with a left-bias on OCT. 15
Figure 12. A. Image Axes; B. the mean intensity profiles; C. the maximum intensity projection profiles 16
Figure 13. (A, B, C)Noise cropping from sample 17
Figure 14. Spheroid selection and fitting using 18
Figure 15. Average X and Z diameters for MCF7 spheroids for different seeding densities 19
Figure 16. Carl Zeiss Axio Observer Z1 Microscope. 22
Figure 17. MCF7 spheroids in different DIVs. 23
Figure 18. Growth of MCF7 spheroids over 7 days 24
Figure 19. Usable Spheroid Quantification. 25
Figure 20. Incubator prototype A 28
Figure 21. Live/Dead Panel 1 31
Figure 22. Spheroid diameter data from FIJI. 34
Figure 23. Plate layouts 36
Figure 24. Zeiss Axiovert 200M Fluorescence Microscope 37
Figure 25. Incubator prototype 2. 39
Figure 26. A. Z-range crop; B. Volume reconstruction contrast mask plots. 41
Figure 27. A representative schematic of spheroid segmentation and selection: A. 2D projection; B. Spheroid selection C. Order of Selection D. top and bottom surface views 3D views 43
Figure 28. A. Spheroids regions for decorrelation, B. Volume by region measurement C. Radius and distance profile graphs for intensity and decorrelation. 45
Figure 29. Average relative changes in spheroid volume in bar and line graphs 48
Figure 30. Spheroid Surface Roughness plots 50
Figure 31. Intensity plots A. by treatment groups; B. by doses in line graph 53
Figure 32. Decorrelation graphs 55

FIGURE 33. COEFFICIENT OF VARIATION (CV) OF DECORRELATION GRAPHS..... 56
FIGURE 34. LIVE/DEAD PANEL 2 58

Supplemental

SUPPLEMENTAL FIGURE 1. COMPARISON OF DIFFERENT IMAGING SYSTEMS AGAINST LEE LAB'S OCT.....64
SUPPLEMENTAL FIGURE 2. SAMPLE DISTRIBUTION FOR EACH EXPERIMENT FOR CELL SEEDING DENSITY.....64
SUPPLEMENTAL FIGURE 3. AVERAGE SPHEROID VOLUMES.....65
SUPPLEMENTAL FIGURE 4. AVERAGE SPHEROID DIAMETER FOR DIFFERENT SEEDING DENSITIES, WITH A DZ VALUE OF 3.5 μM. 65
SUPPLEMENTAL FIGURE 5. MICROTISSUES WITH MCF7 CELLS SHOWING 'CRAWLING OUT' PHENOMENON IN THE SPHEROIDS. 66
SUPPLEMENTAL FIGURE 6. WORKING SOLUTIONS OF PACLITAXEL.....66
SUPPLEMENTAL FIGURE 7. DYNAMIC RANGE MEASUREMENTS (DYN RANGE), SEGMENTATION OPTIONS (OSEG) AND NUMBER OF SPHEROIDS (NS) 67
SUPPLEMENTAL FIGURE 8. AVERAGED ABSOLUTE SPHEROID VOLUMES FOR DIFFERENT TREATMENT CONDITIONS AND EXPOSURE TIMES. 67
SUPPLEMENTAL FIGURE 9. INTENSITY PLOTS SHOWING THE CHANGE IN INTENSITY FOR 0.03 AND 0.3 UM PACLITAXEL DOSES. 68
SUPPLEMENTAL FIGURE 10. THE AVERAGE SPHEROID INTENSITIES (WHOLE, BODY AND CORE) FOR DIFFERENT TREATMENT CONDITIONS AND EXPOSURE TIMES ALL PLOTTED IN THE SAME GRAPH.....69
SUPPLEMENTAL FIGURE 11. RAW INTEGRATED DENSITY PERCENTAGES FOR LIVE/DEAD ASSAY.. 69

Tables

TABLE 1. SCANNING PARAMETERS FOR DIFFERENT OCT SCAN TYPES. ANY PARAMETER NOT INDICATED IN THE TABLE WERE ALLOWED TO STAY AS IN THE DEFAULT/PRESET. 40

Chapter 1

1. Background

1.1 Breast Cancer Research and MCF7 Cells

Breast cancer is the most common cause of death in women between the age of 40 and 65. American Cancer Society estimated that in 2019, approximately 268,600 new cases of invasive breast cancer would be diagnosed, with an estimated 41,760 number of deaths in women[1]. Due to its frequency and impact, breast cancer research has received a lot of attention and has been widely studied at a cellular and molecular level for proper characterization and treatment[22]. Cancer characterization begins in a bench top, with two-dimensional cell culture research in multivariable studies, leading to small and large animal disease models. Cell lines are commonly used element in laboratory research and pertaining to breast cancer research, MCF7 is a popular cell line. The MCF7 breast cancer cell line is a mammalian cell line that was derived from a pleural effusion taken from a 69-year old patient with metastatic breast cancer[3,4]. MCF7 have estrogen receptors, i.e. this is ER positive and exhibits inhibitory responses to antiestrogen treatment[5]. Lippman predicted the future of MCF7 cell line as an important tool for the study of hormone-dependent human breast cancer model. This cell line is being used worldwide and has produced more data than any other breast cancer cell line[2,39].

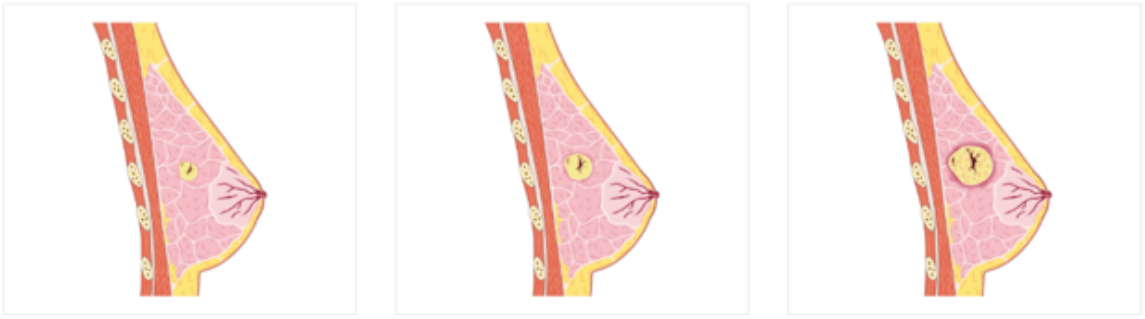

Figure 1. Breast cancer usually begins as a cell cluster (shown as a small yellow ball in the diagram) in one, or both breasts, and experiences significant increase in its volume within a short period of time. Depending on the cancer type, the lump grows well into the chest cavity (not shown) and metastasizes into different parts of the body (Figure created using BioRender).

Just like any other form of breast cancer, this luminal epithelial phenotype cancer begins at the breast as a rapidly dividing and growing cellular structure. The tumor microenvironment plays a major role in the tumor angiogenesis and proliferation, and for years, researchers have been trying to recapitulate the complex tumor microenvironment at a bench-top setup[22,24,28,29]. In this transition of two-dimensional to three-dimensional research, MCF7 has attracted the attention of researchers as a reliable cell line for multicellular tumor spheroids[6,55].

1.2 Three-Dimensional Tissue Research: Microtissues™

For years, scientists have performed in vitro drug testing and have optimized the assays to fit a 2-dimensional platform as the preliminary step towards the research and development of a drug and disease characterization[42]. In vitro cell culture models have been used and optimized widely over the years, 2D cell culture and has been accredited as the gold standard for studying cell behavior *in vitro*. However, these 2D in vitro cell culture models present the limitations of inconsistency, and inaccuracy

depicting the cellular behavior, functions and drug response *in vivo*[7,8,9]. Over the years, cell culture techniques have advanced, and the recent development of 3-dimensional tissue spheroids and organoids can be regarded as the next step towards a more accurate *in vitro* modeling of the cellular environment[32,43,44]. 3D tissue spheroids are considered to nurture an environment conducive to cell-cell and cell-matrix interactions, thereby, mimicking the *in vivo* milieu better in an *in vitro* construct[10, 11]. This is because in a three-dimensional construct, the cells are surrounded by other cells and extracellular matrix (ECM), just like in the body. ECM plays a critical role in the regulation of various biological processes, including cellular differentiation, homeostatic regulation, wound repair etc.[8,12,35]. 2D monolayer fails to recapitulate the complex architecture and specific-to-cell-type composition of the ECM. Therefore, testing any compound in the absence of ECM and the complex cell microenvironment often lead to responses that may not be observed in the true cell milieu.

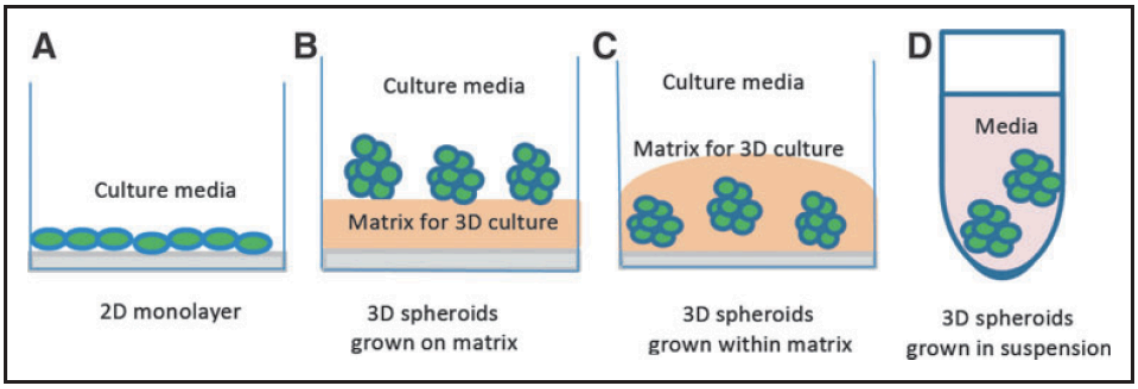

Figure 2. Cell culture in 2D monolayer (traditional) versus different 3D cell culture techniques. B and C both shows 3D cell culture aggregates grown in a matrix-based platform, whereas D depicts cell spheroid growth in a scaffold-free suspension (reproduced from Edmondson et al. review[7])

Realizing the shortcomings of the 2D cell culture and the growing popularity of 3D cell culture, especially in the realm of disease modeling, researchers are increasingly

resorting to different forms of creating 3D cultures[7]. These forms include matrix-based spheroid and organoid growth (on, and embedded) and scaffold-free spheroid formation. Not all 3D culture techniques are ideal, since they include randomized and uncontrolled cell growth, that may inherently have a necrotic core, which would render them unreliable for apoptotic drug studies and disease models[15,21,24,29]. The Morgan lab at Brown University has been investigating 3D cell culture for years, and has utilized the concept of self-assembly to develop the Microtissues^{TM} platform. This is a non-adhesive platform provides a more controlled growth of the 3D cells, and allows them to form structures such as spheroids, honeycombs, toroids etc. Therefore, by controlling different parameters, such as seeding density, one can has a greater control on the size of 3D tissue (or microtissue) being produced for any study[19,20].

1.3 Chemosensitivity and Cell Viability in 3D culture tissues

Cell viability is one of the most important parameters in the cell culture to understand the impact of environmental cues on cell behavior[30]. However, the assessment of cell viability using traditional methods have limitations, especially when used on 3D tissues. Cell viability is usually determined through various invasive assays, that require samples to be discarded upon completion[14,47]. These assays are often tasking and expensive, and despite the hard work, they fail to convey sufficient information about the 3D cell aggregate, simply because most of these assays are not optimized for 3D cell viability assessment[23,29,32]. The invasive nature of these assays also renders them impractical to be used for longitudinal sample monitoring. As fast as the 3D cell culture techniques have improved, the ability to assess cell viability in these samples have not

followed pace in development. In recent years, assays such as CellTiterGlo (Promega), has received accolades for being 3D optimized, however it has not addressed the limitation of longitudinal label-free cell viability assessment[31,33]. This is crucial, in particular, for disease models and drug studies, where the drugs must be monitored over certain exposure times and regimen[34,35]. These assays can also be time sensitive and depend on the penetration rate within a 3D construct[57]. In addition, traditional methods of assessing cellular viability may not be scalable for high-throughput drug screening[26]. Therefore, owing all these limitations, despite the availability of a reliable 3D cell culture platform, assessing chemosensitivity and cell viability can be very challenging.

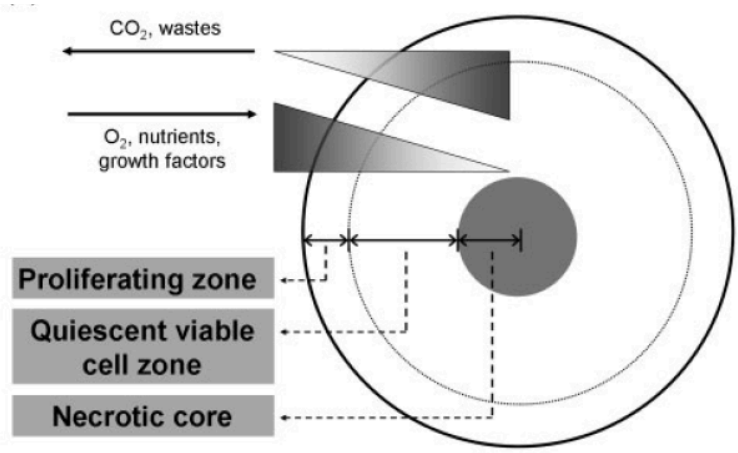

Figure 3. 3D spheroid microenvironment, showing gas exchange, and regions of proliferating, quiescent and dead cells (reproduced from Lin et al.[15])

One assay that is widely used is the Live/Dead assay that uses calcein-AM and ethidium homodimer-1 stains. Intracellular esterase activity converts calcein-AM to fluorescent calcein by hydrolyzing the calcein-AM bond, and outputs a measure for live cells. On the other hand, Ethidium homodimer-1 penetrates damaged cell membranes in

dead cells and binds to the DNA. This stains the dead cells red by enhancing the red fluorescence[63]. This is currently used as a comparable and reliable method of qualitatively assessing cellular viability in both 2D and 3D cells.

1.4 OCT as a Label-Free and Longitudinal Imaging Platform

Imaging techniques have been popularized due to their ability to provide greater details about samples that many invasive assays cannot do. Fluorescence microscopy has been widely for assessing cell viability. With science shifting its focus on precision medicine and patient specific treatments, researchers are turning towards newer optical techniques that are label-free, non-invasive and can provide quantitative results, preferably in real-time[54,56,62]. Optical coherence tomography (OCT) is an imaging technique that has the potential to address those limitations described in the previous section[52,53]. OCT analyzes the interference between the light beam back scattered from a sample and another light beam reflected from a mirror (known as reference mirror). Compared to other emerging optical techniques, OCT can be superior and ideal for 3D tissue culture studies, since it has the ability to acquire images up to single-cell resolution. Supplemental figure 1 shows a comparison between OCT (together with Brown University's Lee lab's imaging and analysis software) and similar optical imaging techniques that are currently being used to obtain information from cells and tissues (in 2D, 3D, *in vivo* and *ex vivo* studies)[14,21,26,32,33,34,35,36,42,45,46,58].

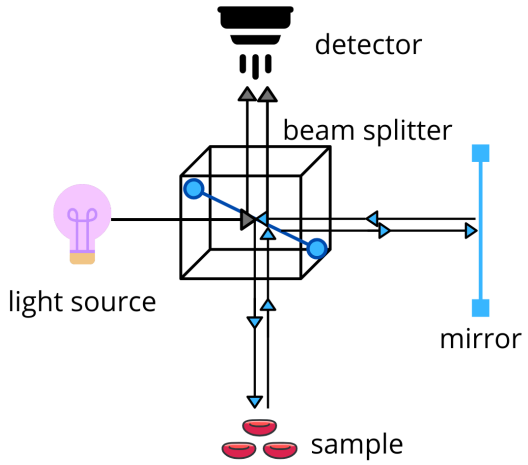

Figure 4. Schematic of time-domain OCT **(created using Canva)**

OCT has been tested previously for its potential to detect changes in cellular movement in 3D neurospheroids in response to ethanol treatment, and therefore it can be expanded to test known drugs in other types of 3D microtissues[48,52,60]. This thesis examines the OCT system's ability to be used to image 3D MCF7 breast cancer spheroids in the context of longitudinal and label-free assessment of chemosensitivity, establishing relevance and necessity in the field of pharmaceutical research and development.

1.5 Choice of Drug: Paclitaxel

Paclitaxel, or Taxol, is a novel plant product and antineoplastic agent that has been isolated from the wester yew, Taxus brevifolia[16]. Studies have reported Paclitaxel to induce objective remission in 56% of patients with metastatic breast cancer[17]. What makes this unique is its mechanism of action[40,50]. While there are various other microtubule interfering agents (such as colchicine and vinblastine), Paclitaxel is

unique in that, it not only promotes microtubule assembly, but also stabilizes the microtubule polymer. This prevents the chromosomes from reaching the metaphase in spindle configuration, and thereby blocks the mitosis progression. This blocking, in turn, triggers apoptosis and reverses the cell cycle to the G0 phase, without undergoing cell division[18]. Paclitaxel and Cisplatin have been the two front-line chemotherapeutic agents that have been tested for their efficacy in three dimensional cellular constructs. It has been reported that Paclitaxel gives MCF7 cells a rounded morphology when treated in 2D and formed small dense ball-like structures in 3D collagen-embedded multicellular spheroids[6]. Extensive literature study has shown that Paclitaxel has been tested widely in MCF7 studies *in vitro*, in both 2D and 3D cells, as stand-alone and combination therapies. Using a known drug to perform a study that would help unveil a technology's potential for cell viability assessment seemed logical[24,28,29]. MCF7 spheroids have been developed and studied, pertaining to the Microtissues^{TM} platform, and therefore, was an ideal candidate for this study. Therefore, MCF7 microtissues, together with Paclitaxel as a treatment, were selected to perform the experiments necessary to prove, or disprove, hypotheses within the scope of this study.

Chapter 2

2. Spheroid Seeding Density Optimization

While MCF7 cells have been widely tested for 3D tissue and spheroid culture, our lab did not have enough experience with this particular cell line, together with the Microtissues^{TM} platform, that provides a more controlled spheroid growth,

unlike traditional 3D cell culture methods. The behavior of these 3D microtissues *in vitro* was important to study in order to decide what spheroid seeding density, drug dose and exposure times would be ideal for testing out the OCT's potential for longitudinal imaging.

2.1 Methods and Materials

2.1.1 MCF7 Cell Culture

Human breast cancer cell MCF7 (ATCC®, HTB-22™; Manassas, VA, USA) were expanded and frozen by previously at Passage-10 (BI 20151230) in 5% DMSO (Fisher Scientific). The cells were thawed and cultured in a Corning T75 (75 cm^2) cell culture flask (Figure 5), in Dulbecco' Modified Eagle Medium 1X (DMEM) (Gibco) (with L-Glutamine) supplemented with 10% Fetal Bovine Serum (FBC) (Gibco) and 1% Penicillin/Streptomycin (P/S) (MP Biomedicals), in a temperature (37°C) and CO_2 (5%) controlled incubator. The cell culture media was replaced every two days, and the cells were cultured for five days, before trypsinization.

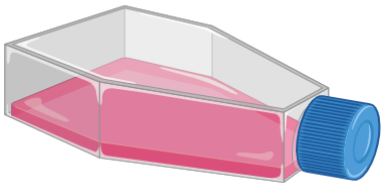

Figure 5. A T75 cell culture flask used for MCF7 cell growth and expansion.

Upon reaching 85% to 90% confluency, the cells were washed with 10 mL warm Versene solution (0.5% EDTA in 1X Phosphate Buffer Saline) once, and then exposed to 0.25% of trypsin solution for 5 minutes. The cells were then quenched with 10 mL of cell culture media (with FBS) to deactivate the trypsin. The flask was agitated, and the entire cell suspension was collected in a 50 mL conical tube. The conical tube was immediately centrifuged at 125 g for 6 minutes. The cell supernatant (Figure 6A) was carefully aspirated out, and the cell pellet was resuspended in cell culture media. The resuspended cells were counted using a hemocytometer (Figure 6B), and about 13,000 cells per cm^2 were transferred to a new 75 flask (next passage). The cells were taken through two rounds of growth and expansion following thawing, before they were ready to form spheroids (described in Chapter 2.1.3).

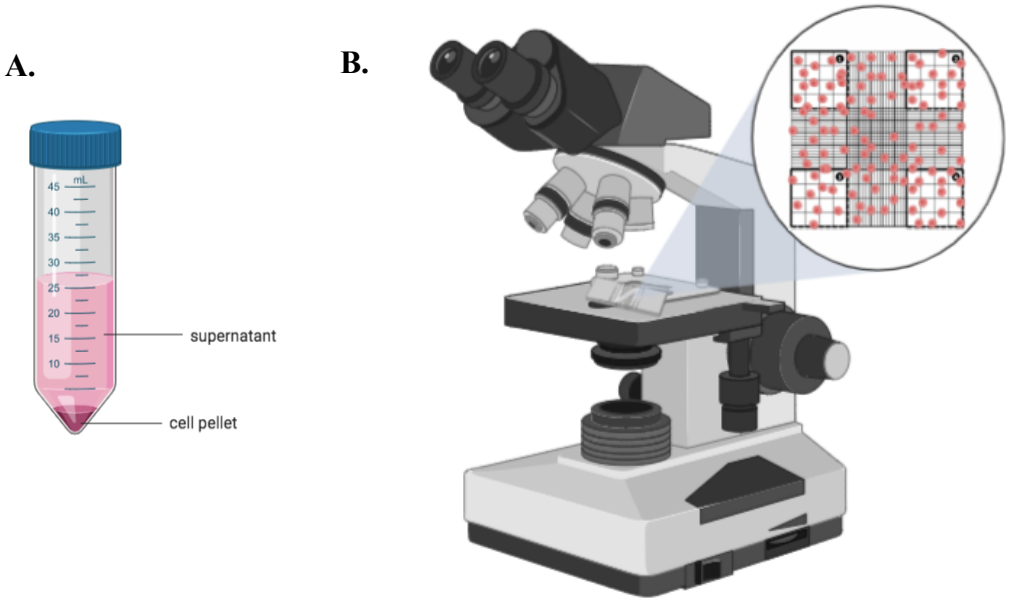

Figure 6. A. A 50 mL conical tube showing the separation of cell pellet and cell supernatant; **B.** A brightfield microscope with a hemocytometer on stage, with a zoomed-in view of the hemocytometer grid with MCF7 cells (shown as red dots) (figure created using BioRender).

2.1.2 Microtissues™: Micromold Preparation

24-96 3D petri dishes were obtained from Microtissues™, that were designed using computer-assisted design (CAD), and fabricated with a ThermoJet® rapid prototyping machine, as described in Napolitano et al.[19]. These 3D petri dishes are silicone negatives, that are used to cast agarose gels, or micromolds (figure 7 and 8A).

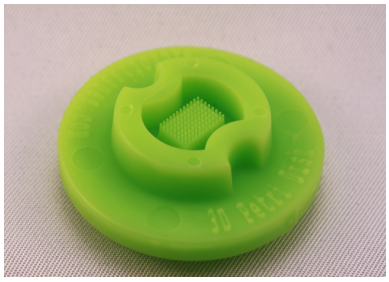

Figure 7. A 24-96 3D Petri Dish (image courtesy: Microtissues, Inc.)

Agarose (Fisher Scientific, BP16-500) was weighed, and autoclaved to sterilize. Theagarose was then dissolved in 1X Phosphate Buffer Saline (PBS) (Gibco), to yield a 2% w/v solution. The mixture was heated using a microwave, until all the agarose fully dissolved. In a sterile laminar flow hood, the molten agarose solution was carefully pipetted into sterile 24-96 3D petri dishes (Figure 8B). All the air bubbles were removed using a spatula, and a flat bottom surface of the micromold was obtained by pressing sterilized coverslips on top of it. The micromolds with molten agarose were allowed to cool. Once polymerized, the excess agarose was scraped off, and the silicone negatives were gently flexed to remove the agarose micromolds (Figure 8C). The agarose micromolds were placed into 24-well cell culture plates, and 1 mL Dulbecco's Modified Eagle Medium 1X (DMEM) (Gibco) (with L-Glutamine) supplemented with 1% Penicillin/Streptomycin (P/S) (MP Biomedicals) was added to each well. The cell culture

plates with the agarose micromolds were carefully taped and taken through cycles of vacuum suction in order to remove any additional air bubbles in the microwell recesses. The micromolds were then equilibrated in 37°C temperature and 5% CO_2 5% controlled incubator for 72-hours prior to seeding.

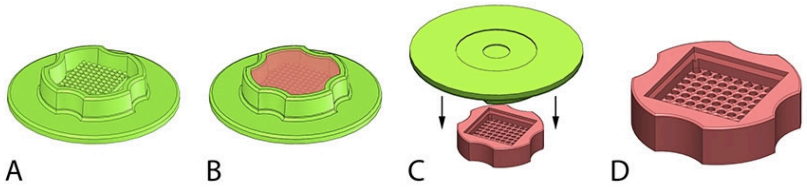

Figure 8. The process of casting a gel-mold using a 3D petri dish (image courtesy: Microtissues, Inc.)

2.1.3 Microtissues Cell Seeding and Tissue Formation

The MCF7 cells in T75 flasks were trypsinized as described in earlier and based on the desired number of cells to seeded per spheroid recess, different volumes of the cell suspension were aliquoted in different 15 mL conical tubes. These tubes were then centrifuged at 800 rpm for 6 minutes, and the cells were resuspended using the desired total volume of cell culture media, with each seeding chamber requiring 70 µL of cell suspension. The resuspended cells were then carefully pipetted into the equilibrated agarose molds, using reverse pipetting technique. For this study, the investigated seeding densities were 250, 500 and 1000 cells per spheroid. Once the agarose molds were seeded, the cell culture plates containing the molds were placed in the incubator for 40-minutes, allowing the cells to settle in the microwells, as depicted in Figure 9 C and D. After the 40-minute incubation, the cells were checked under a brightfield microscope to ensure that the cells were occupying the microwells. To each well containing the

microtissues, 1 mL of warm cell culture media was carefully added, and the plates were placed in the incubator at 37°C and 5% CO2, allowing the microtissues to self-assemble. For this particular experiment, each seeding density had three technical replicates, along with four biological replicates, in order to obtain reliable data.

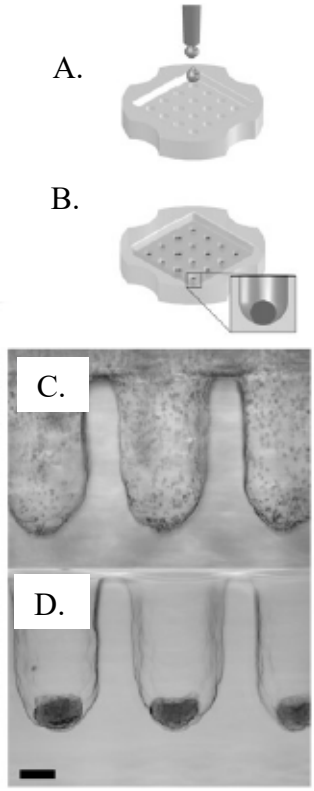

Figure 9. The process of cell self-assembly in Microtissues**: A.** cells are being added to the mold**; B.** cells settle into the microwells under gravitational force**; C.** rat hepatoma cells in micromolds**; D.** cells forming spheroid shapes in the microwells (reproduced from Napolitano et al., 2007[19]).

2.1.4 Tissue Imaging (Seeding Density)

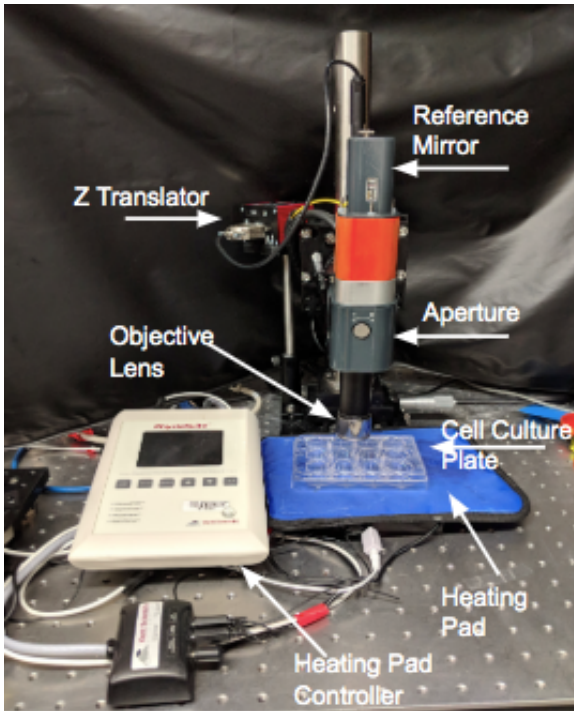

Figure 10. The OCT system set up for a top-down imaging, showing a heating pad beneath the cell culture plate for temperature control.

The microtissues were allowed to self-assemble for 48-hours prior to 3D imaging with the OCT system. Figure 10 shows the experimental setup for this imaging, with the cells being temperature controlled by a heating pad. This was not a sterile setup, since the lid of the plastic cell culture plate had to be removed, in order to image the spheroids with the least glare and light interference. This limitation has been addressed in the following study as described in Chapter 4. Images were obtained using the LSM03 lens, with a 4.6X magnification. The OCT system uses a broadband light with a center wavelength of 1300 nm. The imaging focus was adjusted for microtissues near the center of a gel (shown in figure 11). Each microtissue was first visualized and focused using the

ThorImage OCT 5.2.1 Telesto software, using a field of view (FOV) of 5.12 mm range. Once the microtissue was focused as desired, the ThorImage OCT software was exited out, and the image acquisition was performed using the Lee Lab OCT- 16ThorlabsSD LabView interface, using custom configurations based on the 'Angiogram' preset. Four volumetric scans were taken per microtissue, while repeating 4 B-scans for each cross-sectional plane with a step size of 0.50 mm. The final FOV was 5.12 mm by 10.24 mm. All the microtissues with different seeding densities were imaged the same way, and the acquired images were later 3D-reconstructed using MATLAB and analyzed using Microsoft Excel.

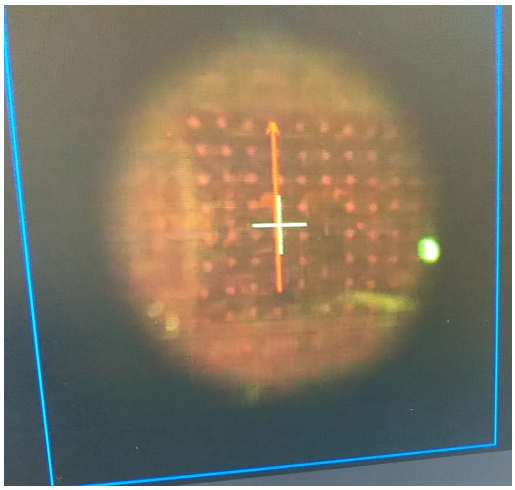

Figure 11. A microtissue focused with a left-bias, instead of the gel in its entirety. This is not desirable, since it does not evenly capture spheroids in the center of the microtissue gel.

2.1.5 Data Reconstruction and Analysis

The data files obtained from image acquisition were reconstructed using the MATLAB code for reconstruction and the reconstructed data was taken through a 'Decorrelation and Geometry' analysis code (cvi-18-cancer/Decorrelation and Geometry) from the Lee lab GitHub repository. Figure 12 A, B and C, show the schematic of the

axes orientation and the mean and maximum intensity projections, respectively, for the image slice shown. The mean intensity projection refers to a set of 2D images are projected into a single 2D image by averaging the values at each position, whereas, the maximum intensity projection depicts a set of 2D images into a single 2D image by selecting the maximum values at each position. The reconstruction code showed the mean intensity and maximum intensity profiles for each image acquired, and showed the position of the spheroids within each microwell. This code also allowed noise cropping for better visualization of the spheroids within the gel (figure 13).

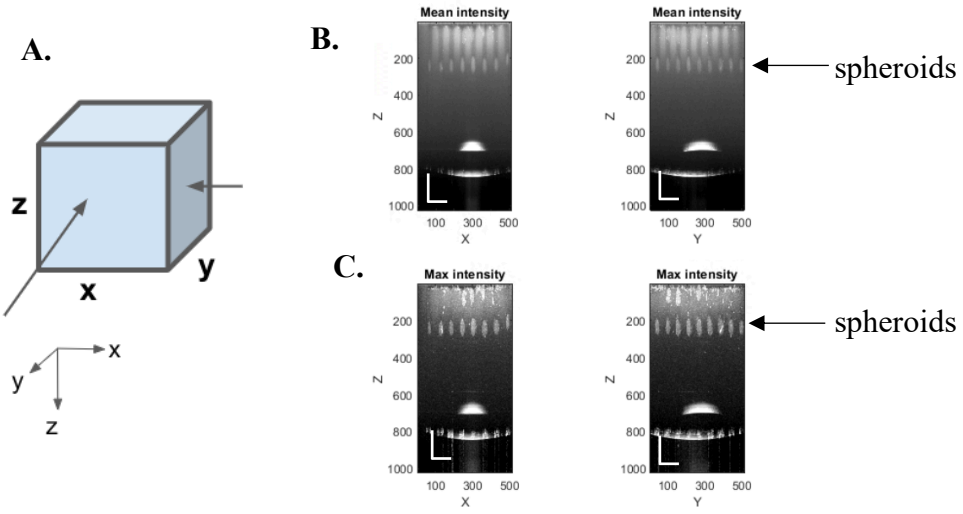

Figure 12. A. A spheroid represented using a cuboid, and the arrows pointing at the direction at which slices B and C are viewed at; **B.** the mean intensity profiles of a microtissue section in X-Z and Y-Z planes; **C.** the maximum intensity projection profiles of a microtissue section in X-Z and Y-Z planes.

Once the images were reconstructed, the code enabled selection of individual spheroids from the 3D image, by setting an ellipsoid-shaped 3D region of interest (ROI) (depicted in figure 14). The code allowed for users to adjust the ROI ellipsoid's center position in 3D, axial diameter, and lateral diameter. For each microtissue per seeding density, 16 spheroids were randomly selected. This code helped obtain the lateral and

axial radii (r_x and r_z, respectively) of each selected spheroid (in pixels), which were later converted to micrometers by using the imaging voxel (3D pixel) size. The lateral sizes of the imaging voxel (d_x and d_y) were set to 10 µm as input during image acquisition). Initially, the theoretical value of the axial voxel size (dz = 3.5 µm) was used. Then, the volume of the spheroids was calculated using an ellipsoid volume formula (Equation 1).

$$\boldsymbol{Volume\ of\ Spheroid = \frac{4}{9}\pi[2(r_x)^3 + (r_z)^3]}\ \textbf{(Equation 1)}$$

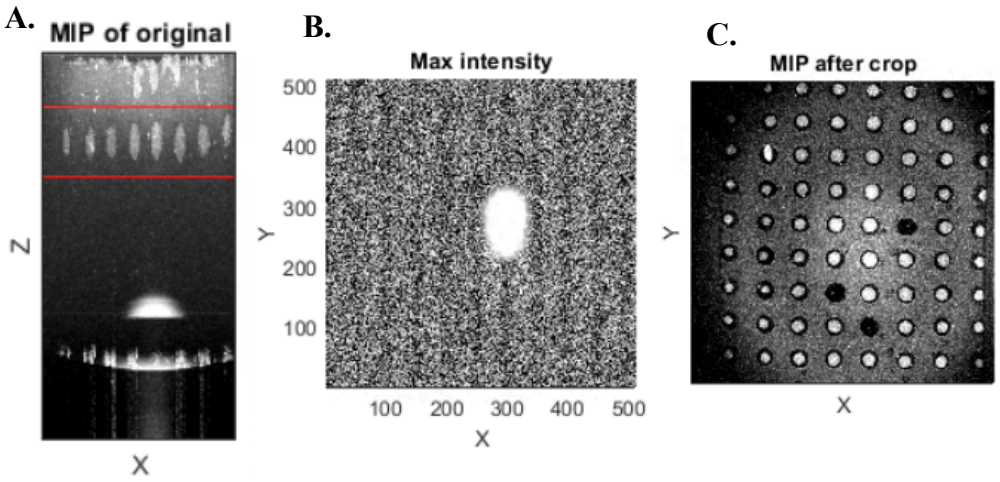

Figure 13. A. Spheroids shown as bright ellipsoids, and the red parallel lines indicating the selection of the spheroids within the microwell; **B.** maximum intensity XY profile before cropping (bright white spot corresponding to the glare at the bottom of the XZ profile); **C.** XY intensity profile after cropping- the white circles refer to the spheroids within each microwell, and the black circles refer to empty wells.

The results obtained for each round of experiment were reconstructed and analyzed in the same process, and the obtained values of volume, x-diameter and z-diameter were averaged over spheroids. Any outliers outside two standard deviations were eliminated for the later statistical analysis. Significance was demonstrated using a paired student's t-test.

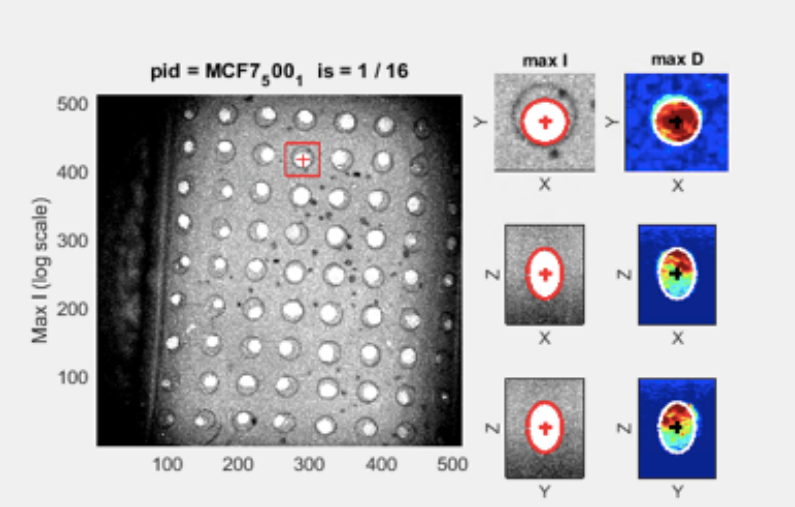

Figure 14. Spheroid selection and fitting using the 'Decorrelation and Geometry' analysis code. Max I profile shows the selected spheroid in each plane, and the Max D profile shows a heat map showing motion within the spheroid in each plane.

2.2 Results and Discussion

Results showed that the volume increased as the spheroid density increased (Supplemental figure 3), as expected. This experiment was also showed that MCF7 cells did not form exact spheroids but formed ellipsoids. Initially, the *dz* value was assumed to be 3.5 µm for the *CRz* radius conversion, however, the assumed value yielded z-diameter values much larger than the x-diameter (about 100 µm higher than expected, shown in Supplemental figure 4). This indicated the need for calibrating the OCT's voxel size in z-axis, using 355-425 µm polystyrene beads. Hence, we performed an additional experiment with Barium Titanate and Sala Lime glass beads and analyzed 16 beads to give a new *dz* value of 2.88 µm (procedure and results not included). Figure 13 shows the average x and z diameters for spheroids with 250, 500 and 1000 cells per spheroid seeding densities with the new *dz* value, post-calibration. As expected, the spheroid

diameter displayed significant increase when the seeding density increased. The OCT was effective to capture these size changes.

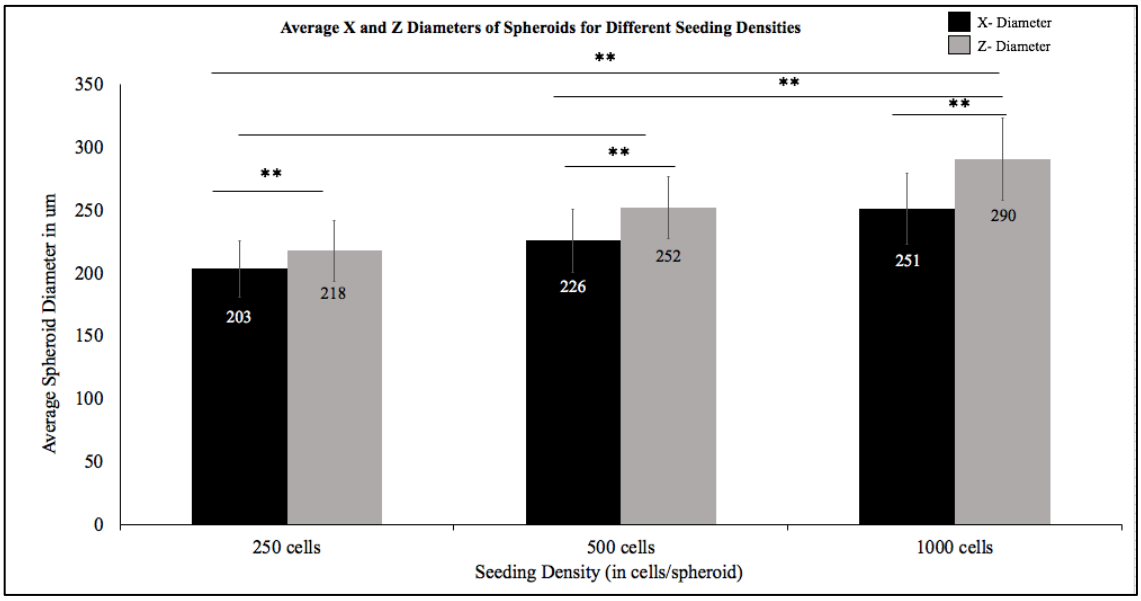

Figure 15. Average X and Z diameters for MCF7 spheroids with 250, 500 and 1000 cells/spheroid seeding densities. The asterisks indicate statistical significance with p-value< 0.01. The diameters were significantly different for all seeding densities, for both X and Z axes.

One key observation we made during this experiment was the 'crawling out' phenomenon of the MCF7 spheroids. Supplement figure 5 shows a brightfield image snapshot of the MCF7 spheroids at DIV 2 with three different magnifications. MCF7 spheroids were seen to attach to the microwell walls and displayed the tendency to propel themselves out of the microwells. This was a constant observation throughout the entire experiment, particularly notable in higher seeding densities. This experiment initially tested seeding densities of 500, 1000, 2000 and 3000 cells/spheroid, but most of the spheroids at higher seeding densities were seen to have crawled out of the microwells by DIV 2. Therefore, we adjusted the testing range to 250, 500, and 1000 cells/spheroid as presented. Kosaka et al. (human hepatoblastoma), Enmon et al. (human prostate), Fehlauer et al. (human glioma), Sutherland et al. (mouse and human colon carcinoma) all

performed extensive study showing that as the spheroid diameters get larger than ~200 μm, the oxygen uptake declines, which in turn, has an impact how cells respond to drugs. In conclusion, our results showed that a spheroid seeding density of 250 cells/spheroid have the average x and z diameters closest to 200 μm., suggesting that this seeding density is suitable for the following studies described in Chapters 3 and 4.

Chapter 3

3. MCF7 Proliferation *in vitro*

Most literature study referred to Ki67 proliferation marker as an ideal end-point study for MCF7 cells (usually in 2D), and while MCF7 cells are known to proliferate rapidly, their proliferation rate using the Microtissues^{TM} 3D platform was not studied in the past. In order to perform an effective longitudinal anticancer drug study, it was crucial for us to identify the starting time for the drug treatment, and the duration of the drug exposure. These starting time and drug exposure duration may depend on the critical DIV at which the MCF7 spheroids would have proliferated to the point of 'crawling out' of the microwells while in culture media. Since the culture media would be a control group for the experiment, crawling out of spheroids would make it extremely difficult to accurately quantify the spheroid geometry metrics such as the volume and surface area. And hence, we studied the growth and proliferation of MCF7 spheroids *in vitro* for seven days, before conducting an anticancer drug study.

3.1 Methods and Materials

3.1.1 Cell Culture and Tissue Formation

MCF7 spheroids were fabricated using the microtissue molds as described before, in sections 2.1.1-2.1.3. Only one seeding density (250 cells/spheroid) was tested for this in vitro proliferation study. Briefly, MCF7 cells grown in a T75 flask was allowed to reach 85% confluency (Day 5). 24-96 small spheroid micromolds were made using 2% molten agarose (in PBS), and equilibrated using FBS-free culture media. MCF7 cells were trypsinized and resuspended, and the resuspended cells were used to seed the equilibrated micromolds. The spheroids were allowed to self-assemble overnight, and the spheroids were imaged for DIV= 1, 2, 3, 5, and 7. The tissue media was changed on DIV= 3 and 5, prior to image acquisition. A total of four microtissues were seeded for each round of the experiment, and the experiment was repeated three times, before obtaining average values for results.

3.1.2 Longitudinal *in vitro* Imaging

Once the microtissues were allowed to self-assemble, the tissues were imaged using widefield microscopy, with Carl Zeiss Axio Observer Z1 microscope, connected to an AxioCam MRm camera (Carl Zeiss MicroImaging, Thomwood, NY), with a Zeiss imaging and processing software (Zen Pro with Zen Light for image processing). The software enabled the capturing of the complete microtissue with a 5X magnification, and each microtissue was focused prior to the capture. The acquired images were saved as both .czi and .tif formats. The software performed automatic

stitching and enabled viewing each microtissue in its entirety. MCF7 microtissues were imaged at a temperature and CO2 controlled compartment (shown in figure 16), and once imaging was complete, the cell culture plate with the microtissues were placed in a 5% CO2 and 37°C controlled incubator and allowed to grow.

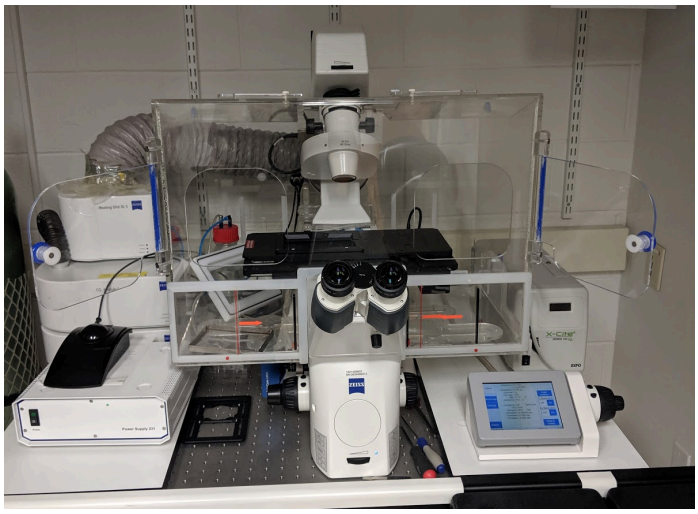

Figure 16. Carl Zeiss Axio Observer Z1 Microscope used for longitudinal proliferation imaging.

3.1.3 Data Analysis: FIJI

FIJI software version 1.0 was used to load the .tif images obtained from the Zen Pro software, and spheroids were selected such that 40% of the selected spheroids were from the edge of the microtissue, and 60% of the selected spheroids were from the center of the microtissue. For each DIV, 20 spheroids in total were selected, and the same spheroid was tracked for all the DIVs in consideration. The diameters of the spheroids were measured using the 'Straight' line function on FIJI, and the data obtained were analyzed using MS Excel. The images were converted to 16-bit prior to obtaining the data, and the scale was set at the same value for all the images (a 1000 µm scale bar was added to each image using the Zen Light software, and using that scale bar, the scale

was set with a pixel ratio on FIJI). Since the same spheroid was tracked over time, a paired t-test was implemented to asses significance. The diameter values of all the spheroids were averaged for each experiment, and the results from all three experiments were averaged to give final diameter values for the spheroids. The asterisks indicate a P-value< 0.05.

3.2 Results and Discussion

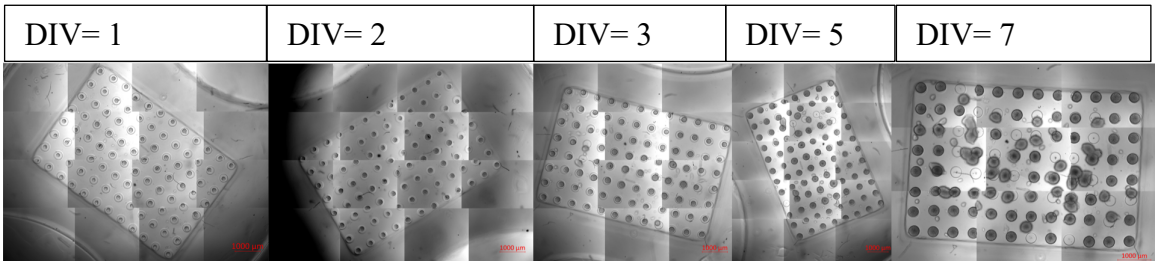

Figure 17. The same microtissue with MCF7 spheroids imaged at DIV= 1, 2, 3, 5 and 7, with 5X magnification. Visually, spheroids on DIV= 7 look significantly larger and more crawled out compared to DIV= 1. Scale bar shown on the image= 1000 µm.

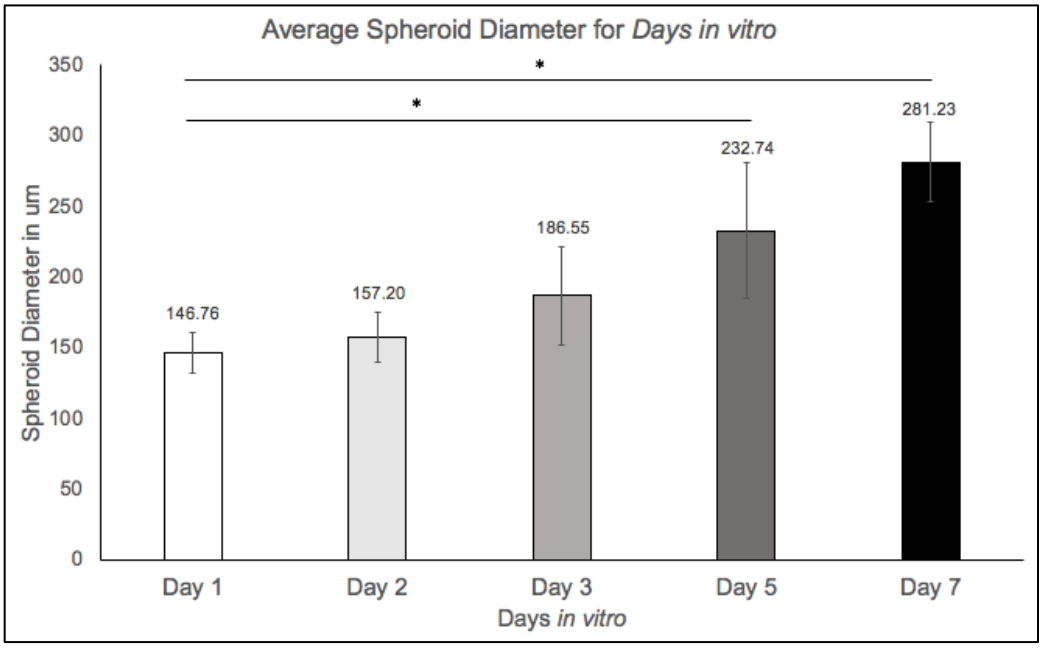

Figure 18. Growth in MCF7 spheroids over seven days, interpreted from changing spheroid diameters (measured in μm). Number of spheroids analyzed= 20, and data from three experiment rounds were averaged to give the final spheroid diameters, shown above. The asterisks indicate P-value< 0.05.

Figure 18 represents growth and proliferation of MCF7 spheroids, expressed in terms of change in average spheroid diameter over the days *in vitro*. Results show that the spheroids underwent growth and proliferation for all seven days in culture, and the most significant growth occurred after DIV= 3. Therefore, based on this result and aforementioned literature, we designed the following anticancer drug study (Chapters 4 and 5) that the spheroids are exposed to anticancer drugs within DIV= 1, 2 and 3. The significant increase in spheroid size observed at DIV= 5 and 7 may make it difficult to detect and interpret possible differences in spheroid size between the control and experimental groups in the anticancer drug study.

The phenomenon of 'crawling out' may be more challenging than the physiological proliferation. Thus, we determined whether individual spheroids crawled out, at each DIV. In detail, using the 'Multipoint' function of FIJI, the spheroids within the microwells (usable) and the spheroids outside of the microwells (not usable) were identified and numbered. We found that as the days *in vitro* increased, the number of usable spheroids decreased (Figure 19). With 96 spheroids per gel, an average of 22 spheroids crawled out of the microwells by day 5 in culture media. To keep more than 75% of the spheroids usable, we decided to avoid DIV 5 in the following anticancer drug study. This DIV criterion was consistent with that based on the proliferation (Figure18). In conclusion, we decided to use DIVs 1-3 for the anticancer drug study.

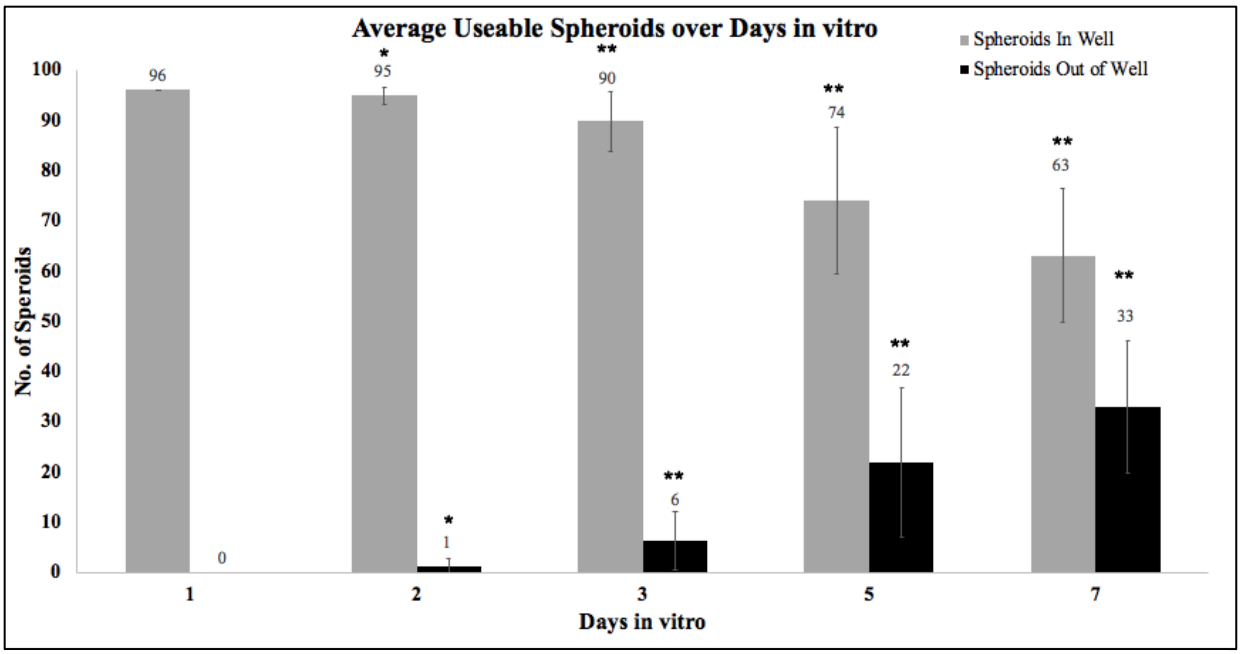

Figure 19. Average number of spheroids in a microwell (grey) and number of spheroids out of a microwell (black) for different DIVs, quantified using FIJI. Single asterisks indicate p-value< 0.05 and double asterisks indicate p-value< 0.01.

Chapter 4

4. Dose-Time-Response Study using Paclitaxel:

Pilot

Once we had determined the spheroid seeding density for the study, it was important to understand the effect of the drug of our choice on the microtissues. 3D tissues behave differently than 2D cells grown in cell culture plastic. Even though we have literature references showing how 3D cell clusters react to Paclitaxel[22,27,30,36,38,39,40,41] those studies did not utilize the same 3D tissue growth

platform that we were using. Hence, it was important to conduct a pilot study to understand the dosage of the drug and how the spheroids in microtissues would react to this widely studied drug. This experiment helped us establish the protocol for conducting an *in vitro* viability study using OCT imaging, followed by Live/Dead assay for method validation.

4.1 Method and Materials

4.1.1 Cell Culture, Drug Treatment and OCT Imaging

MCF7 microtissue spheroids were fabricated and seeded at 250 cells/spheroid seeding density and allowed to self-assemble for 24-hours, as described previously. Two sets of gels were prepared for each experiment: one plate for OCT imaging and a second plate for Live/Dead cytotoxicity assay. OCT plate was designed to have four treatment conditions: one media control and three different doses of paclitaxel. The Live/Dead plate was designed to have five conditions: one media control, one 70% ethanol control, and three different paclitaxel doses. Each condition had technical duplicates for both OCT and Live/Dead assay. Paclitaxel (Cell Signaling Technologies, MA) was reconstituted in dimethyl sulfoxide, DMSO (Fisher Scientific), to make 1 mM solutions and stored as 55 µL in DNA/RNA free PCR tubes at -20°C. Supplemental figure 6 shows the tabulated form of the working solution preparation, and for each experiment all the working solutions were made fresh from a 1 mM paclitaxel solution aliquot and sterile DMSO stock. For this pilot study, 2 uM, 0.2 uM, 0.02 uM paclitaxel concentrations were used for treatment, and the study was an end-point assessment study. The OCT images were acquired in a top-down setup (shown in figure 10), using the same

scan and imaging protocol as described in section 2.1.4.

4.1.2 Live/Dead® Viability Assay

To assess cellular viability, Live/Dead® cytotoxicity kit for mammalian cells (Thermofisher) was used. The kit contained 4 mM Calcein-AM (for viability) and 2 mM ethidium homodimer-1 (for cell death), and the kit was sealed and stored at -20°C, away from light, until the assay was performed. Prior to starting the assay, cell culture medium was aspirated from two wells with microtissues and 1 mL of 70% etOH was added to both. All other wells containing microtissues were taken through three rounds of washes using serum-free medium (DMEM with Penicillin/Streptomycin), with ten minutes incubation (in a temperature and gas-controlled incubator). This was done to ensure that the serum esterase activity was quenched before adding the Live/Dead reagents.

Calcein-AM and ethidium homodimer-1 reagents were thawed in the dark to room temperature and were briefly pulse centrifuged at 1000 rpm for 8 seconds. To the same conical tube with serum free medium, Calcein-AM stain was added to yield a 2 µM solution, and ethidium homodimer-1 stain was added to produce 4 µM solution. Upon careful removal of the media and 70% etOH from the wells with microtissues, 1 mL of the stain mixture was added to each well. The plate was then covered with aluminum foil and incubated in a temperature and gas-controlled incubator for 30-minutes.

Once the incubation period was over, the plate was imaged using the Zeiss Axio Observer Z1, described in section 3.1.2. XCite fluorescence lamp (series 120 Q) was warmed up for 15-minutes and was used to provide fluorescence illumination at the EGFP (green) (488 nm excitation peak, 509 nm emission peak) and dsRed (558 nm excitation peak, 583 nm emission peal) channels. The exposures were kept identical for all the microtissues in similar conditions (an average of 82 milliseconds for EGFP 400 milliseconds for dsRed), and the media control (live) and EtOH (dead) microtissues were used to establish the exposure times for live and dead stains.

4.2 Results and Discussion

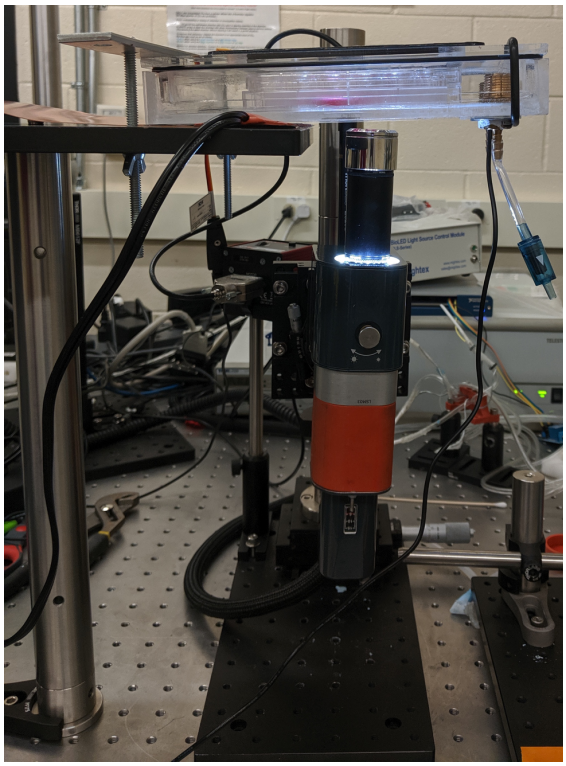

Figure 20. Lee lab's first incubator prototype, set for bottom up imaging using the LSM03 lens. Inside the incubator is a plastic bottom 24-well plate containing MCF7 spheroids treated with Paclitaxel.

The field of view used for OCT image acquisition for this study was 5.12 mm by 10.24 mm, and therefore, each experiment with technical duplicates generated too large data to be processed by the current computational capacity of the Lee Lab. This lesson from the pilot study helped us better design the OCT imaging parameters in the main anticancer study as described in Chapter 5.

This pilot experiment also allowed for testing a *custom-built incubator in progress* (figure 20). Since this study focused on the OCT's ability to be established as a platform for longitudinal drug study, it was crucial to have an experimental setup that would enable spheroids to be in a controlled environment during the duration of drug treatment, minimizing any external influence on cellular viability. Experiences and feedback from this pilot study were applied to the final instrumentation of the incubator.

This pilot study also helped us develop the best practices for bottom-up spheroid imaging using the OCT. Even though the spheroids were visible using a 24-well standard plastic-bottom plate, the glare was relatively high, and the spheroids were difficult to focus. Even when the spheroids were visible, the intensity (visually) was far lower than observed when performing top-down imaging. This established the need for using glass-bottom plates, and it also confirmed that the design process of the incubator for the drug study was effective for a bottom-up imaging setup. Only temperature and gas-control mechanisms had to be put to use for the incubator, as well as the design of the incubator was being worked upon by Ahbid Zein-Sabatto for easier assembly and disassembly.

We also identified that tilting the OCT scope at a certain angle helped further eliminate glare, occurring from light bouncing off of the well wall and aided focusing the spheroids even if a microtissue gel was not of the highest quality (for instance, there may be agarose debris producing unwanted shadow), or the volume of the culture plate well may not be suitable for good spheroid viewing. Even though this caused the acquired image to show the microwell at an angle, this technique still helped us capture the whole microtissue.

Finally, this pilot study enabled us to re-adjust the spheroid seeding density for clearer OCT imaging. The previous chapters suggested that the density of 250 cells/spheroid may be the best in the context of the spheroid size and crawling out. However, this pilot experiment revealed that a seeding density of 250 cells/spheroid was not ideal for OCT imaging. This lowest density produced spheroids that were difficult to focus, despite employing the aforementioned troubleshooting techniques. The image produced from 250 cell/spheroid seeding density was also difficult to analyze, since the spheroid shape was less ellipsoidal when viewed in 3D. Figure 19 showed that 90% of spheroids did not crawl out at DIV 3 when the seeding density was 250 cells/spheroid. As we decided not to exceed DIV 3, it is expected that 70-90% of spheroids (at least 50%, conservatively) would not crawl out at DIV 3 when the higher seeding density of 500 cells/spheroid is used. Therefore, we decided to use 500 cells/spheroid in the following anticancer drug study as described in Chapter 5.

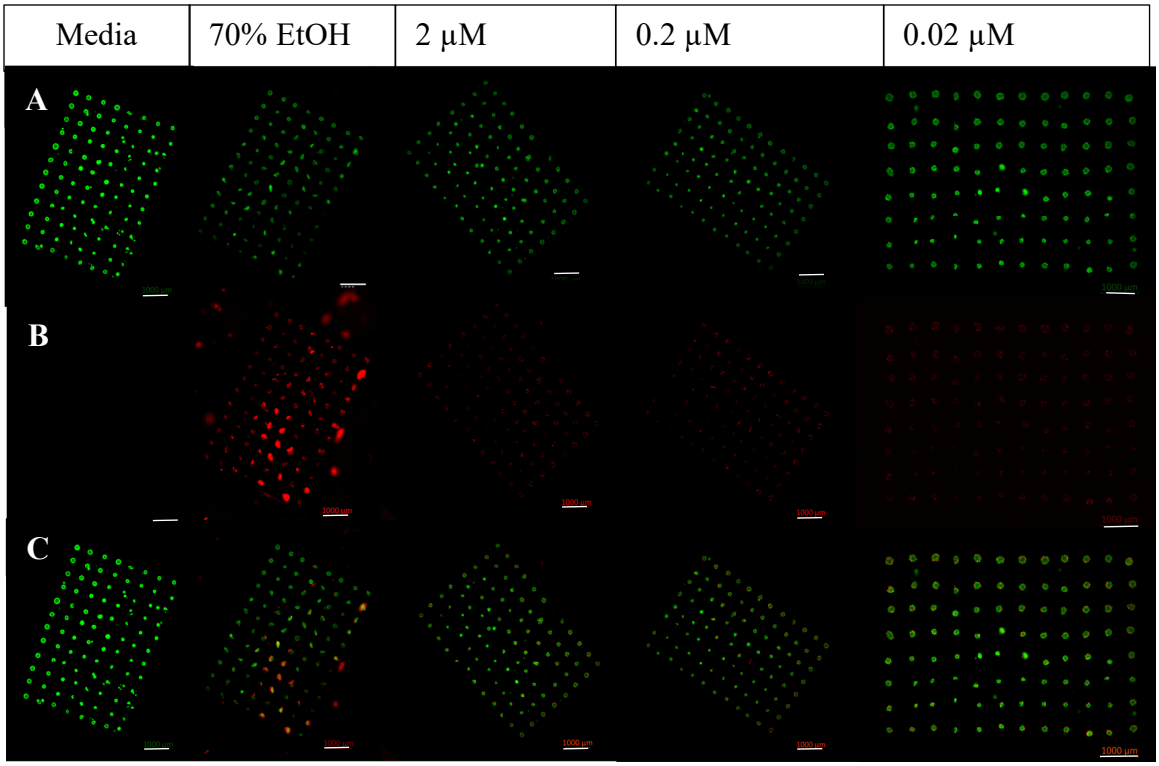

Figure 21. A representative panel of live, dead and combined images of MCF7 spheroids after 24-hours of paclitaxel exposure. Cells were mostly viable in the drug treated groups (green channel- row A), and the dead cells were certainly difficult to see (red channel- row B). Images were acquired for green, red and brightfield (not shown). Scale bar= 1000 µm.

This pilot study helped us establish procedures of conducting the Live/Dead viability assay of MCF7 spheroids. While the EGFP (green channel) was much easier to view, the dsRed (red channel) was much more difficult to focus. This experience underlined the importance of the microscope condenser, and how to eliminate a lot of the debris that contribute to the noise in the image (Figure 20 row B 70% EtOH image is a good example). The debris, agarose and cell clusters, often make it difficult to identify the true signals, giving raise to false positive values. Benjamin Wilks (Morgan lab) provided useful feedback at this stage of the experiment on how to produce better quality images for Live/Dead assay analysis. Ethidium homodimer-1 has a different working

mechanism than Calcein AM, and therefore a 30-minute incubation time after adding the stain solution may not have given a better view of the red channel. Therefore, we increased the incubation time to be 40-minutes after adding the stain solution for the main study. Visually, the dsRed fluorescence was certainly highest at the negative control for the assay (70% EtOH). The dsRed fluorescence was also higher for the higher concentration of paclitaxel, compared to a lower concentration.

The pilot Live/Dead assay helped us identify and fix an experimental mistake. When designing this pilot study, we did not accurately take into account the dilution of media from the microtissue mold, which might make the result show less dead cells than expected in the drug treatment groups. The microtissue mold is composed of 98% media and 2% agarose, after they have been equilibrated. Therefore, diffusion of small molecules occur between the media (with drug) and the volume inside the microtissue mold. This happens relatively quickly to equalize the concentration in the well. In this pilot experiment design, the 24-well agarose mold together with the seeding chamber had the total volume of 0.39 mL, and 1 mL media with the drug was added to each well. Therefore, the 1X concentration of the drug added was not the true concentration being supplied to the spheroids. And therefore, we realized that the drug dosages must be increased to 1.39X for the spheroids to receive true 1X concentration in the main study.

Since the Zeiss Axio Observer microscope enabled brightfield image capturing simultaneously with the fluorescence imaging, the brightfield images from this experiment were analyzed using FIJI 1.0 software, as described in section 3.1.3. The

primary observation of paclitaxel treatment was that the MCF7 spheroids were seen to dissociate from a solid sphere to individual cell aggregates. Even though the direct comparison of a solid spheroid to a spheroidal cluster of individual cells may not be accurate, it was important for us to observe how the spheroid diameters varied across different conditions. Data from three experiment rounds were collected and analyzed, and the spheroid diameters were found to be significantly different between media control, paclitaxel treatment groups of 2 μM and 0.2 μM doses and 70% ethanol treated control. The average spheroid diameter was found to be the highest for 70% ethanol treatment group, since the MCF7 spheroid were notably swollen when treated with ethanol. This finding was consistent with our previous findings where neurospheroids were treated with ethanol. In contrast, the spheroids treated with high-concentration paclitaxel (0.2 uM and 2.0 uM) exhibited significant decrease in size. Those treated with the lowest concentration (0.02 uM) did not exhibit any significant size difference from the media control group. However, this data was obtained from 2D brightfield images that do not provide sufficient information about the spheroids in their 3D microenvironment. This data only reassures the need for OCT's ability to provide more in-depth information about the spheroids in their 3D milieu.

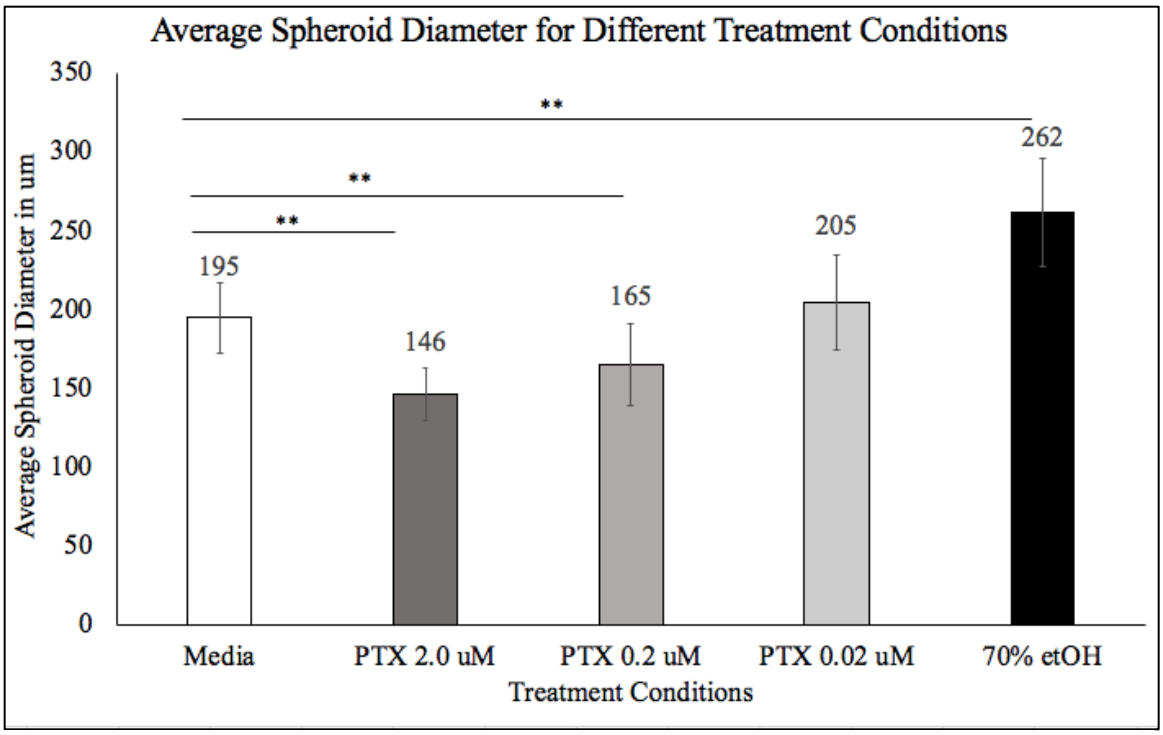

Figure 22. Average spheroid diameter calculated using FIJI from brightfield images. 16 spheroids were selected from each microtissue of each condition, and data obtained from three experiments were averaged to give the final values. The asterisks indicate p-value<0.01.

Chapter 5

5. Dose-Time-Response Study using Paclitaxel

This study utilized all our previous findings to test the OCT together with a new mini-incubator prototype, for longitudinal imaging of MCF7 spheroids treated with Paclitaxel. This study had the potential to provide us with information about the same set of microtissue samples over a 24-hour time period, unlike our previous end-point studies. This is particularly crucial to prove that OCT can suffice as a label-free platform and is reliable like the Live/Dead viability assay.

5.1 Methods and Materials

5.1.1 Cell Culture, Spheroid Formation and Drug Treatment

MCF7 cells of the same batch (as earlier experiments) were thawed and cultured for two passages prior to seeding in microtissue molds. For each experiment, the microtissue molds were made fresh and equilibrated for 72-hours in serum free media. The cells were seeded to form spheroids with a seeding density of 500 cells/spheroids, and the spheroids were allowed to self-assemble for 24-hours. The microtissue molds were placed in glass-bottom plates (Gamma irradiated, sterile; MatTek Corporation, MA) and the spheroids were cultured in the glass-bottom plates to eliminate the need for microtissue transfer from one plate to another. Paclitaxel dilutions were made similar to the pilot study, however, factoring in the 1.39X dilution, the new concentration for the doses were 3 μM, 0.3 μM and 0.03 μM. Each treatment condition was plated in technical duplicates, and the entire experiment was identically performed for three times. The spheroids were treated with paclitaxel for 24-hours, and OCT images were acquired prior the addition of the drug (pre-treatment), 12-hours and 24-hours after the treatment was started. The media control used for the experiment was MCF7 cell culture media (as described in Chapter 2.1.1) with DMSO (concentration <0.05%, keeping consistent with the concentration of DMSO with all drug treatment groups).

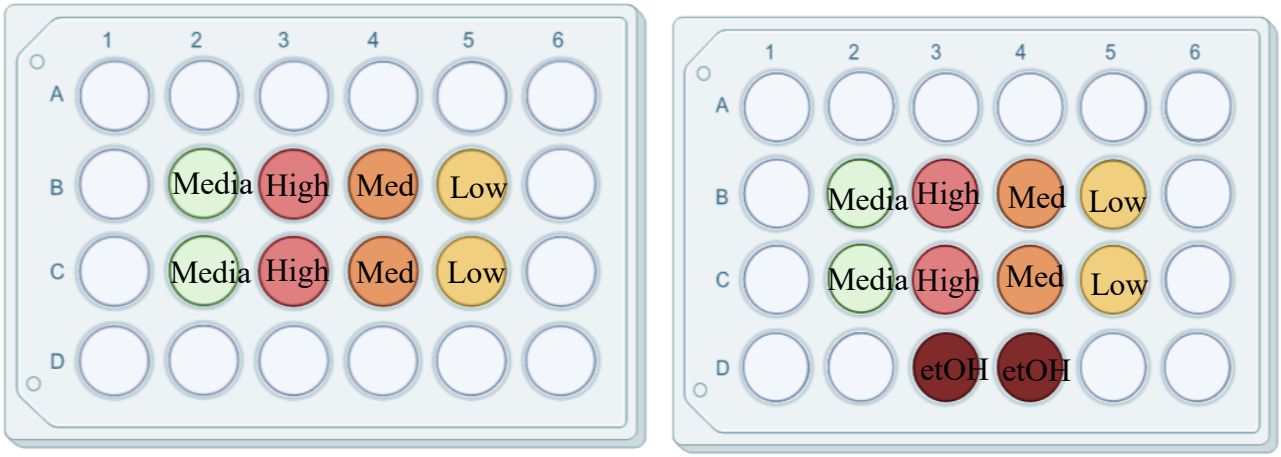

Figure 23. (left) Plate layout for OCT longitudinal study; **(right)** plate layout for Live/Dead assay. High, Med and Low correspond to 3 uM, 0.3 uM and 0.03 uM concentrations, respectively. The OCT plate did not have a control for cell death due to limitations in imaging window.

5.1.2 Live/Dead® Viability Assay and Imaging

Since Live/Dead assay requires samples to be stained, this viability assay was only performed at the end of the 24-hour mark. Live/Dead assay was executed as described in Chapter 4.1.2, and the cell culture plate was incubated for 40-minutes (in a temperature and gas-controlled incubator) prior to imaging.

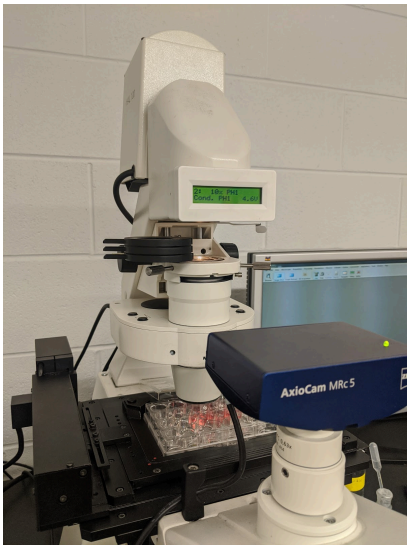

Figure 24. Zeiss Axiovert 200M Fluorescence Microscope with the condenser head off.

After the incubation was over, images were acquired using Zeiss Axiovert 200M Fluorescence Microscope (figure 24), connected to a camera and computer with AxioVision Rel.4.8 software, for image viewing and acquisition. Unlike the Zeiss Axio Observer Z1, the AxioVision does not have the capacity to automatically capture the microtissue gel in its entirety at a 5X magnification, i.e. no automatic image stitching. Therefore, each well had to be imaged between 6 to 9 times in different positions to manually capture the entire microtissue. This process was time consuming and required the spheroids to be exposed to fluorescence light for a longer period of time. Hence, the fluorescence strength was kept between 50 to 65% for all the experiments to prevent sample bleaching. The condenser was adjusted to eliminate background noise and interference from debris. The microtissues were focused at Phase-I of the and acquired using a customized multidimensional acquisition channel definition. For the realm of this experiment, the EGFP channel (green, for viability) was set with the FITC hardware setting, and the dsRed channel (red, for death) was substituted with TRITC hardware

setting. The wavelengths were slightly different for TRITC compared to dsRed, and therefore, the exposure time was adjusted to account for this difference. The TRITC channel was never allowed to go above an exposure time of 800 millisecond to prevent acquiring false positives. Brightfield images were acquired simultaneously along with the fluorescence images. The images were always viewed on 'Linear' at the Scope Orca interface of the AxioVision software to see the raw data, as they were captured. All the images were saved as. zvi to prevent data loss. For quantitative analysis, Raw Integrated Density (RID) values were measured for individual spheroids from the fluorescence images obtained. Multiple codes were created to aid automatic background masking and RID quantification (FIJI- Benjamin Wilks, Julian Montagut; MATLAB- Ahbid Zein-Sabatto) did not work well, this quantification was performed manually using FIJI by creating an ellipsoidal selection to collect background noise for each channel separately, and then the same ellipsoidal selection was used to select individual spheroid within the image. The pixel area, integrated density and raw integrated density values were measured. The data was then collected on a MS spreadsheet, and the background was eliminated for each channel.

5.1.3 Longitudinal OCT Imaging using a Mini-Incubator

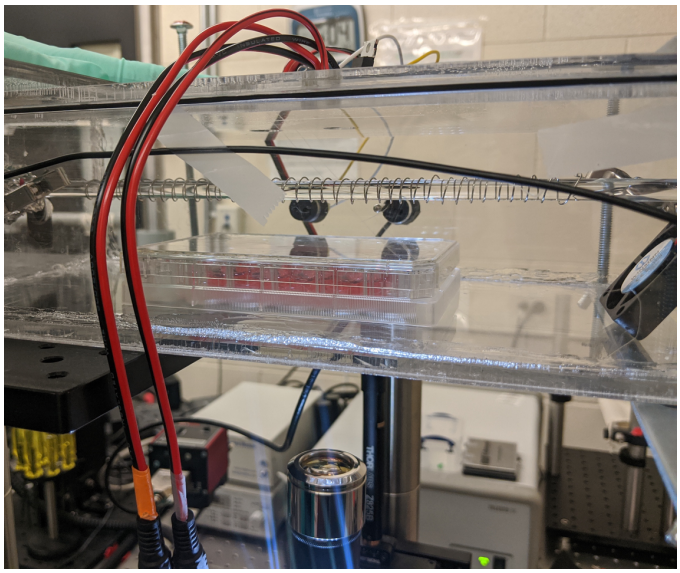

Figure 25. Incubator prototype 2 (side view), with even temperature control using a feedback circuit for heating mechanism, and a micro-fan for even heat distribution. This incubator has the potential for gas control, but gas control was not available for this experiment.

For allowing longitudinal imaging with the bottom-up setup, the cell culture plate was placed inside the mini incubator prototype (figure 25) for the entire duration of the experiment. The spheroids were imaged prior to starting the treatment (pre-treatment), and then the plate was removed from the incubator to a sterile cell culture hood and paclitaxel was added to wells, as established in the protocol. Once the drug was added, the cell culture plate was placed back in the mini incubator, and images were acquired again at 12-hour time point and 24-hour time point after drug addition.

Each microtissue was imaged three times for three different scan types- decorrelation, attenuation and dynamic light scattering (DLS). The spheroids were focused, viewed and captured as previously described. According to the lesson obtained in the pilot study, the field of view was reduced to 2.56 mm from 5.12 mm. Decorrelation

and attenuation scans were performed using the 'Angiogram' preset and DLS scan was performed using the 'DLS LSM03' preset with the parameters listed in table 1.

Scanning Parameter	Decorrelation	Attenuation	DLS
Repeated B-scan number (*bpy*)	4	4	preset value
Voxel size in Y (*dy*)	10	10	20
Voxel size in X (*dx*)	10	10	10
Number of volume scans (*nv*)	4	4	preset value
Number of voxels in Y (*ny*)	256	256	128
Number of voxels in X (nx)	512	512	preset value
***MX*)**	preset value	preset value	128
Voxel size in X for DLS in mm (*x-step*)	preset value	preset value	0.02
Flyback time	preset value	preset value	0.0025

Table 1. Scanning parameters for different OCT scan types. Any parameter not indicated in the table were allowed to stay as in the default/preset.

The images acquired were longitudinal since the same samples were imaged over time.

5.1.4 Data Reconstruction, Segmentation, and Analysis

The data acquired were reconstructed using the Lee lab's MATLAB code *1 Reconstruct* under the *2003c* branch of the *fpm-1-metric* repository. The reconstruction process was similar to the described previously, and figure 26 A shows how the code enabled noise cropping (at z-range). This code, however, had a bug; thus, the reconstruction was conducted again with a fixed code *temp2003d filter intensity.mlx* that applied a filter to produce clearer intensity images and lower the variations in values. Figure 26 B shows the decorrelation and intensity images, where the intensity image is very clear, post intensity filtering.

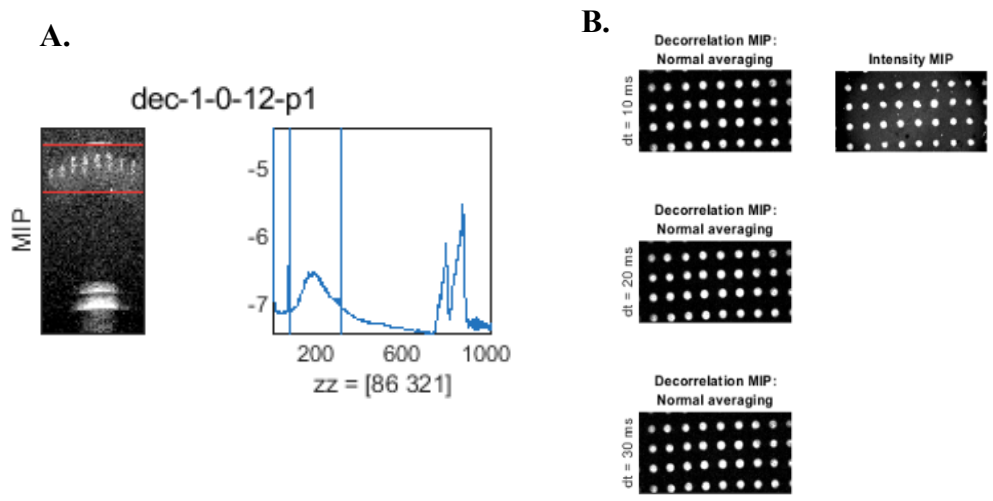

Figure 26. A. Z-range crop**; B**. reconstructed volume and contrast-masked average plots for three decorrelation time points (10 ms, 20 ms, 30 ms), and the intensity image.

Once the data were reconstructed and filtered, *2 Segment Spheroids* code was used to select spheroids from MIP images for further analysis. This code enabled viewing the *en face* representative slices of each loaded sample and perform and automatic segmentation of spheroids. The dynamic range of the spheroids was manually entered during this step of the data analysis process. The dynamic range is an important parameter, that refers to the fraction of darkest or brightest voxels that get ceiled or floored for further image processing. Altering the lower limit of this range can make spheroid voxels darker and produce spheroids that appear bumpier than they really are. The upper limit of this range saturates the spheroid voxel brightness and may increase the noise. The dynamic range was entered such that the background (agarose mold) was dark enough, without impacting the brightness of the spheroid/cell clusters, while viewing the result in real time as a feedback. Supplemental figure 7 shows a tabulated form of the

dynamic range, segmentation options and the number of spheroids selected for analysis for this study.

The segmentation code also provides four segmentation options for morphological image processing. These options produce spheroids with different levels of erosion, and the selection of this option varied from dataset to dataset. For each data point, different number of spheroids were selected. Selecting spheroids in the same order for all time point would refer to longitudinal data analysis, but for this study, spheroids were not selected in the same order since the microtissues were left free floating the media (not glued down), and because the mini incubator had a fan for temperature control, it was difficult to image the same microtissue with the same orientation for all time points. Therefore, the selecting the same spheroid for analysis would not necessarily correspond to the same spheroid in the actual experiment. Figure 27 A depicts the OCT XZ-plane view of the spheroids for one of the pre-treatment microtissues, and 27 B shows the spheroids post-segmentation. This code interface enabled viewing spheroid selection order (27 C) and also top and bottom views of the spheroids in a 3D interactive plot. This plot can be moved to different orientations to ensure all the selected spheroids were ideal and did not have any additional noise or debris (figure 27 D has one spheroid visible in both top and bottom views that contains additional noise).

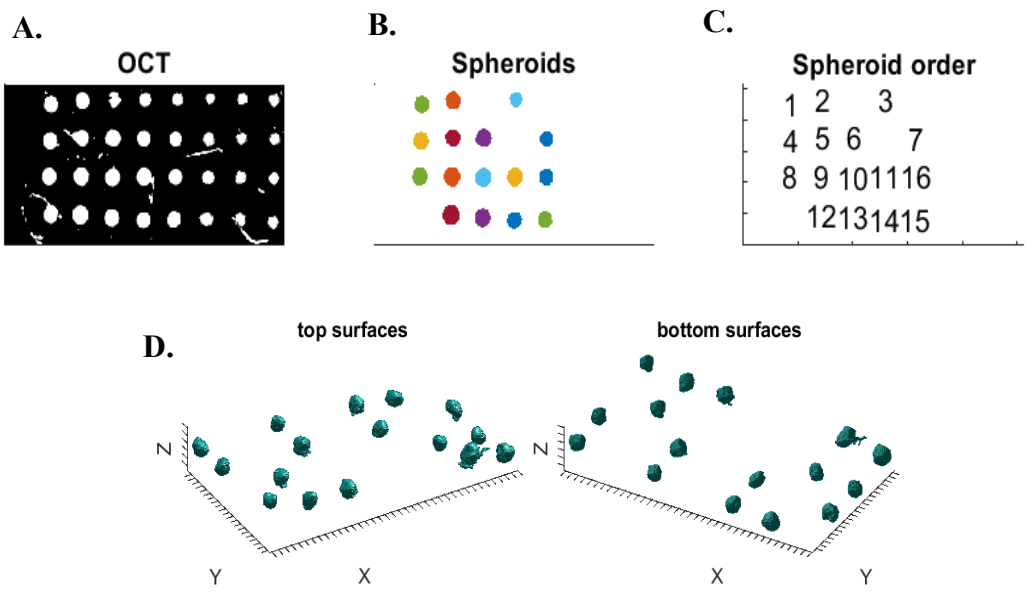

Figure 27. A representative schematic of spheroid segmentation and selection: **A.** 2D projection of spheroids from the reconstructed data from OCT, **B.** Selection of different spheroids and **C.** the order in which the spheroids were selected. This feature allowed the selection of the same spheroid in the same microtissue over time, **D**. top and bottom surface views of the segmented spheroids in an interactive 3D map. This interactive 3D map allowed viewing of each spheroid from both top and bottom views, and any spheroids with additional debris were identified at this stage, and the code was re-ran to select a different spheroid.

Once the spheroids were segmented for all data points, the segmented data were analyzed using *3 Measure Geometry* code. This code allowed the input of the drug exposure times (0, 12 and 24 hours in this case), and yielded the spheroid volume (in μm^3), area (in μm^2), the area to volume ratio, and a spheroid surface roughness. The surface roughness (SR) metric was defined by the formula in equation 2.

$$\boldsymbol{Surface\ Roughness} = \frac{\left(\frac{a}{4\pi}\right)^{\frac{1}{2}}}{\left(\frac{3v}{4\pi}\right)^{\frac{1}{3}}} \quad \boldsymbol{where, a = area;\ v = volume}$$ **(Equation 2)**

SR is independent of the spheroid size, and it assigns a value of 1 to a perfectly smooth sphere, and as the sphere surface gets rougher, the value increases above one (can

measure up to 10 μm or one-cell depth). This is a better measure compared to the area to volume ratio since it allows a relative comparison between samples.

The intensity and decorrelation of the samples were then measured using the 4 Measure Intensity and Decorrelation code. This code defines each spheroid over 12 regions: whole, shell, body, core, top-whole, top-shell, top-body, top-core, bottom-whole, bottom-shell, bottom-body, and bottom-core (figure 28 A). This code also presented the intensity and decorrelation profiles as a function of the distance from the center (i.e., radius) or the distance from the surface. For this study, the B-scan was repeated 4 times with 10 millisecond time intervals as shown in Table 1; thus, it generated three decorrelation maps with time intervals of 10, 20 and 30 ms). The results obtained from MATLAB analysis were grouped according to time points (because this study had technical duplicates for each treatment condition) and averaged to give values for the desired metrics. The data obtained were then taken into MS Excel and analyzed to produce desired diagrams and statistical tests.

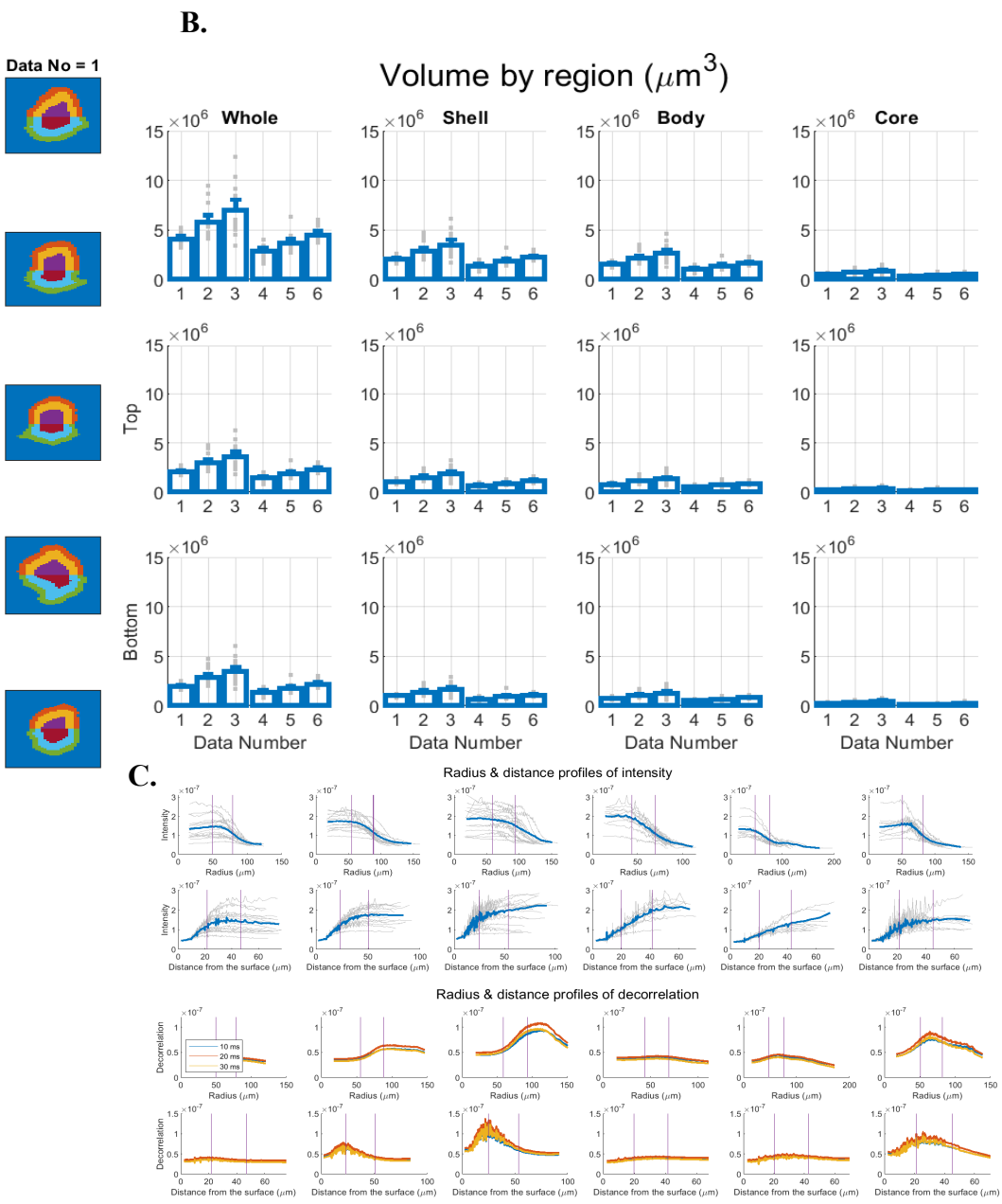

Figure 28. A. Spheroids showing the 12 different regions taken into account for decorrelation and intensity measurements, **B.** Volume by region measurement graphs for the spheroid, **C.** Radius and distance profile graphs for intensity and decorrelation.

5.2 Results and Discussion

5.2.1 Geometry

Maintaining consistency with our previous studies involving MCF7 spheroids, we first looked at the changes in spheroid volumes and how they can capture spheroids' response to paclitaxel treatment. To focus on the drug response rather than absolute volume values, we normalized the volume values to the pre-treatment value for each condition, and then plotted normalized spheroid volumes for different exposure times and treatments. We labeled each condition:

Ctrl0: Spheroids in media before starting the treatment;
Ctrl12: Spheroids in media (adjusted with EDTA) at 12-hour;
Ctrl24: Spheroids in media (adjusted with EDTA) at 24-hour;
L0: Spheroids in media before starting the treatment;
L12: Spheroids in 0.03 μM Paclitaxel at 12-hour;
L24: Spheroids in 0.03 μM Paclitaxel at 24-hour;
M0: Spheroids in media before starting the treatment;
M12: Spheroids in 0.3 μM Paclitaxel at 12-hour;
M24: Spheroids in 0.3 μM Paclitaxel at 24-hour;
H0: Spheroids in media before starting the treatment;
H12: Spheroids in 3 μM Paclitaxel at 12-hour;
H24: Spheroids in 3 μM Paclitaxel at 24-hour;

Our previous result in Figure 18 showed that the spheroid volume did not significantly change until DIV 3. However, when compared between each group, we found that there was an increase in volume observed (see Ctrl0-Ctrl24). Since there was significant change in volume observed, we began close monitoring of the mini incubator temperature (via webcam, that allowed remote access as well), and also performed an

additional test to asses whether the lack of gas control contributed to this change (explained in Chapter 6).

We plotted this fold in volume change of the spheroids against Paclitaxel doses in order see whether we obtained a traditional downward moving curve, testing whether spheroid volume as a metric can be regarded as a direct measure for cell viability or chemosensitivity. This is because, since Paclitaxel is an antiproliferative drug, our initial hypothesis was that it would be able to stop the growth and proliferation of the MCF7 spheroids. Unfortunately, the volume curve was upward trending and plateaued quickly. This could have resulted from the disaggregation of the spheroids in response to the drugs[39]. Since the spheroids were no longer retained their shapes and disaggregated into individual cell (and cell clusters), the analysis code may have considered the entire region the cells occupied, and thus provided numbers reflecting an increased volume. Even though we noticed changes in cellular volume for the same treatment group over time, with metric did not show any significant change in spheroid volume due to an increasing dug dose. For future studies, we could include higher drug concentrations up to 30 μM[21] to examine any significant changes pertaining to spheroid volume. Supplemental figure 8

shows the absolute spheroid volume values, represented in treatment condition clusters.

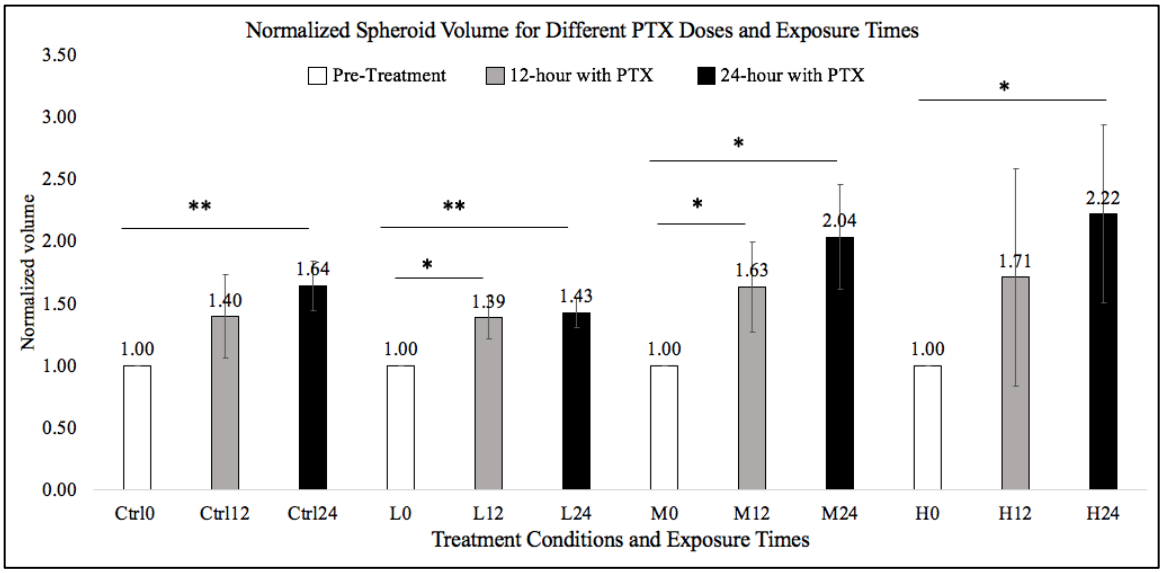

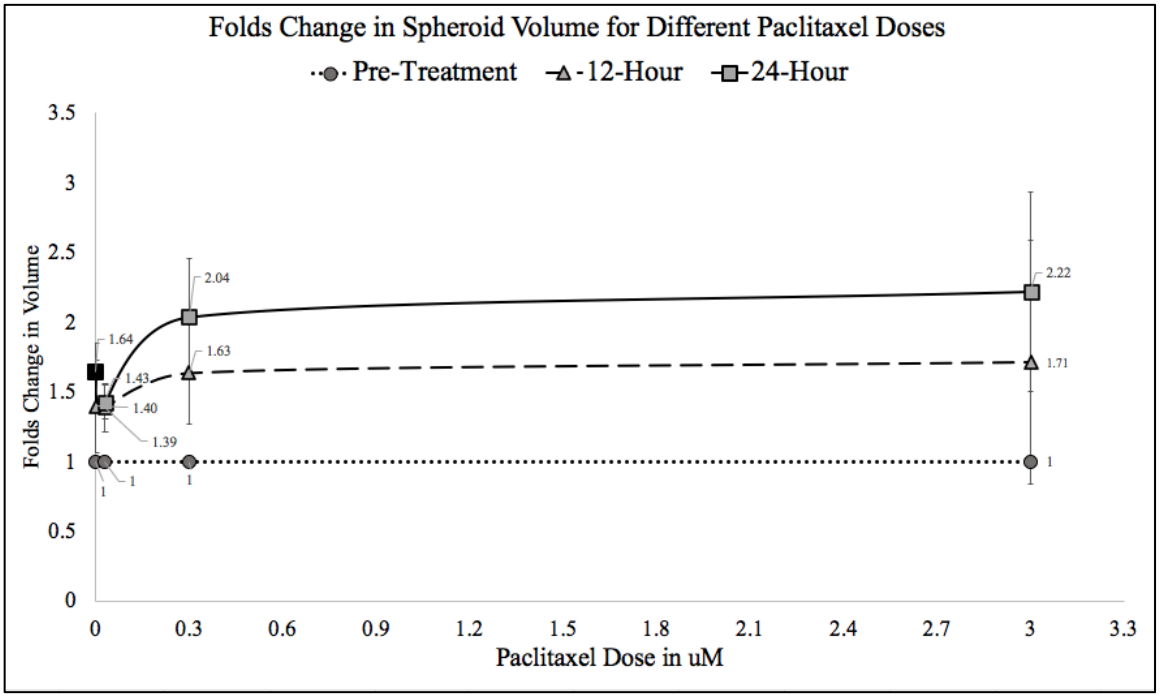

Figure 29. (top) Average relative changes in spheroid volume represented in treatment group clusters, for different exposure times. Since the values for each group was normalized to its pre-treatment microtissue, all the columns for exposure time 0 (pre-treatment) is 1. Single asterisks indicate p-value< 0.05 and double asterisks indicate p-value< 0.05.
(bottom) Average relative change in spheroid volume represented in a line graph: dotted line corresponds to pre-treatment (hence, reads 1), dashed line corresponds to 12-hour after exposure and solid line represents 24-hours after exposure.

Since spheroid volume as a metric did not provide sufficient information to distinguish between spheroid growth and cell death-oriented volume change, we examined if the surface roughness is a better predictor of morphological changes in MCF7 spheroids. The higher the surface roughness, the bumpier a spheroid is. Since visually most spheroids appeared disaggregated in the drug groups, it was expected that the surface roughness would be significantly higher in the highest Paclitaxel concentration group. However, that was not the case (Figure 30). One possible reason behind this could be a bias in the manual selection of spheroids during the segmentation process. We selected segmentation options such that spheroids look more even. This bias, however, may mean that we were prematurely eliminating bumpier spheroids that could have given us significant changes in surface roughness values, which may let us have missed the opportunity of capturing evidence that surface roughness is indeed a reliable metric to assess cellular viability.

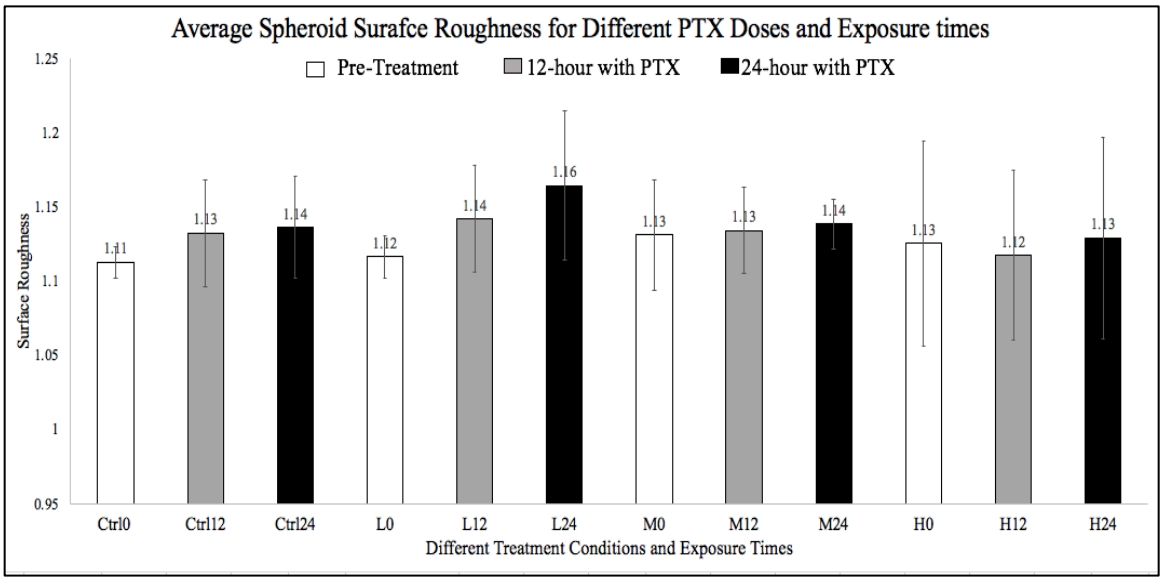

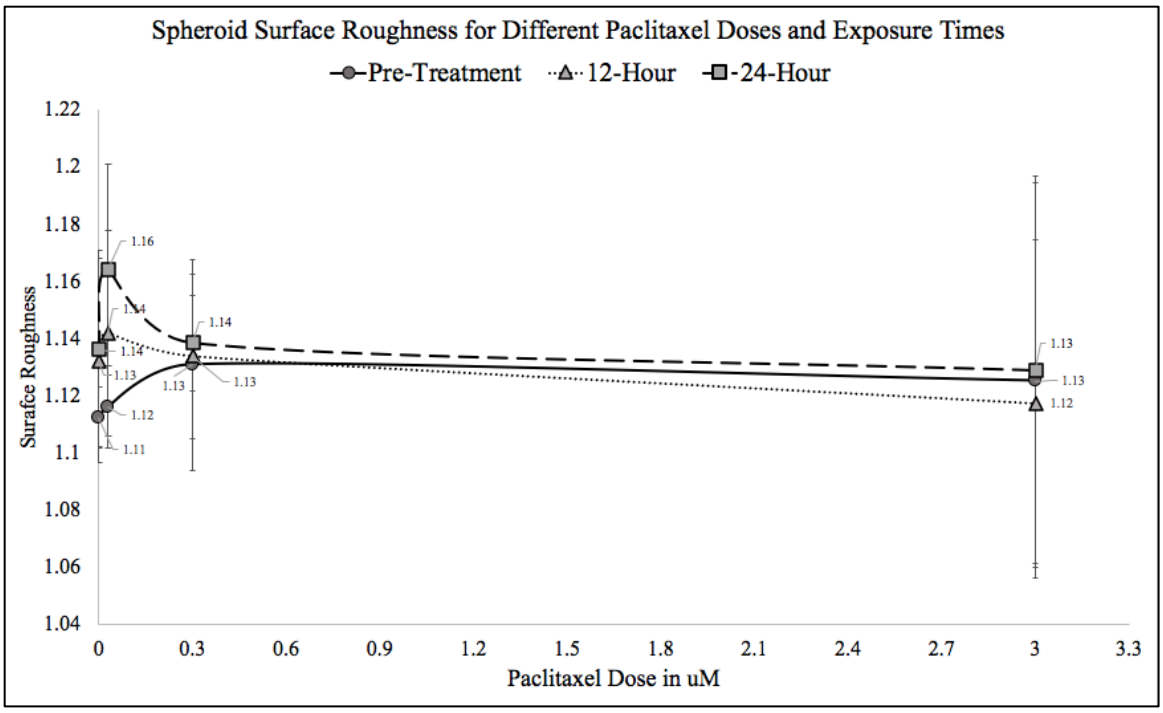

Figure 30. (top) Spheroid Roughness categorized by treatment groups and exposure times. No significant difference was observed between any groups; **(bottom)** Spheroid surface roughness plotted against different paclitaxel doses for different exposure times. Only a slight increase in surface roughness was observed for all treatment conditions.

5.2.2 Intensity and Decorrelation

As explained earlier, each spheroid was divided into 12 different regions for intensity and decorrelation analysis. For the purpose of this study, we only present results from three regions: the whole spheroid, spheroid body, and the core of the spheroid. We did not take the spheroid shell into consideration in this analysis, since the shell is the boundary between the medium and cells where the optical intensity and decorrelation signals often become less robust. Initially, the intensity data was grouped for all the different treatment group, for whole, body and core (of the spheroids selected), and the average data was plotted to observe any notable trends, relevant to typical dose-response curves (figure 31B). There was a slight decline in intensity observed for higher

drug doses at 24-hour, however, the values were not statistically significant. However, when average intensities were plotted as Whole-Body-Core clusters for different treatment groups (supplement figure 31A), it was observed that the intensity values at the spheroid core were consistently high for all treatment groups and exposure times. Even though the results were not statistically significant, the fact that intensity was the highest at the spheroid core made us think how the amount of backscattered light may dictate cellular viability. Looking at our previous Live/Dead data, we noticed that the live stain was prominent at the spheroid core. This meant that intensity perhaps corresponded to the number of live cells within a spheroid, instead of dead cells. In order to validate whether this method worked, and whether the results obtained from the OCT data was reliable, the experiment findings were compared to the Live/Dead assay findings.

A.

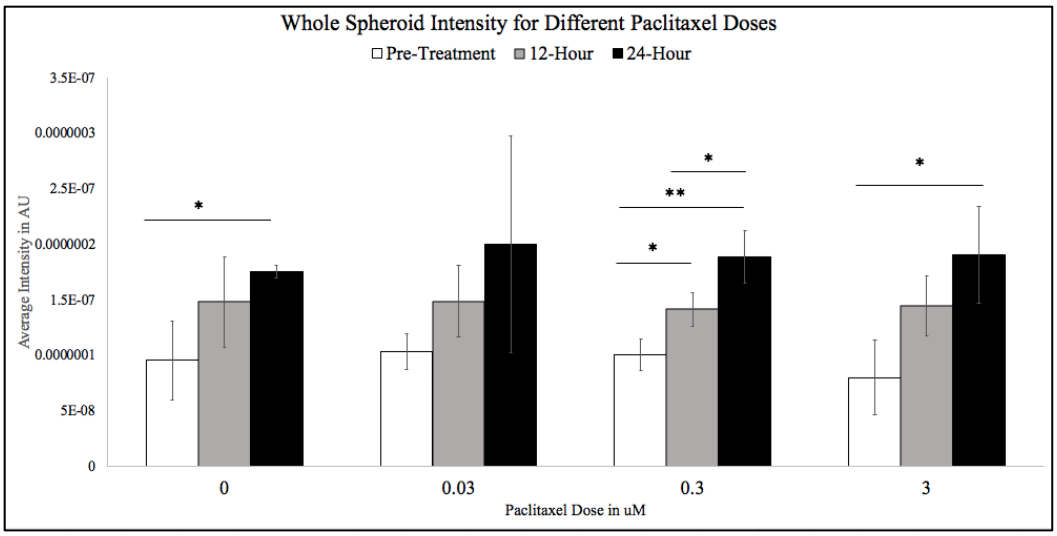
Whole Spheroid Intensity for Different Paclitaxel Doses
Pre-Treatment
12-Hour
24-Hour
Average Intensity in AU
3.5E-07
0.0000003
2.5E-07
0.0000002
1.5E-07
0.0000001
5E-08
0
0
0.03
0.3
3
Paclitaxel Dose in uM

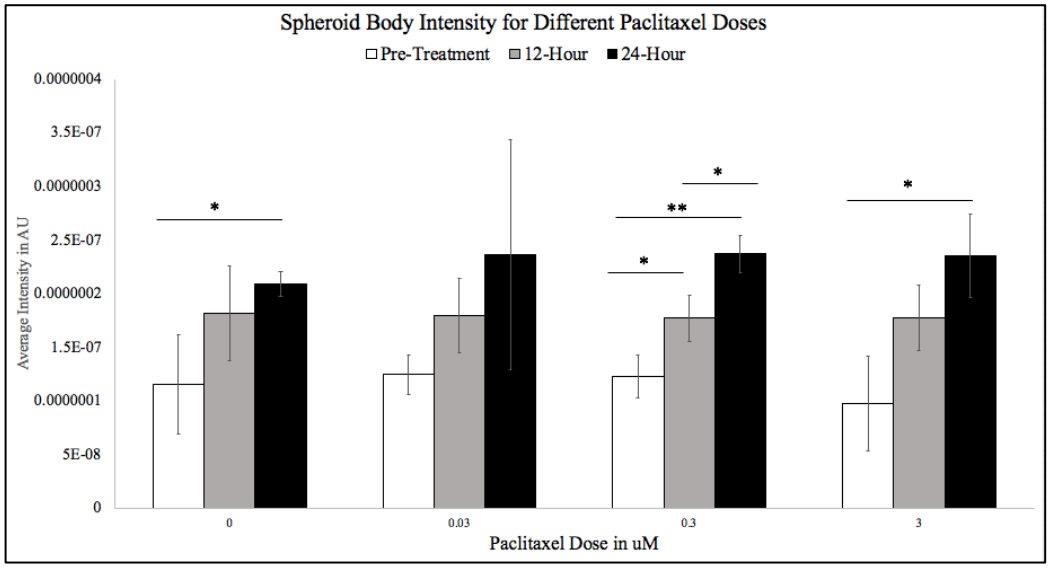
Spheroid Body Intensity for Different Paclitaxel Doses
Pre-Treatment
12-Hour
24-Hour
Average Intensity in AU
0.0000004
3.5E-07
0.0000003
2.5E-07
0.0000002
1.5E-07
0.0000001
5E-08
0
0
0.03
0.3
3
Paclitaxel Dose in uM

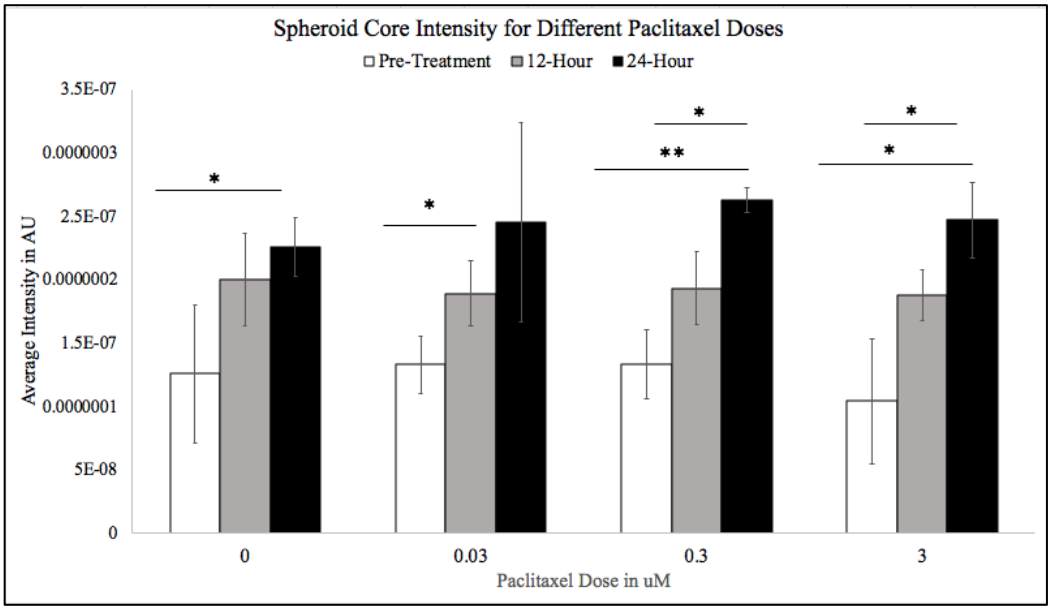
Spheroid Core Intensity for Different Paclitaxel Doses
Pre-Treatment
12-Hour
24-Hour
Average Intensity in AU
3.5E-07
0.0000003
2.5E-07
0.0000002
1.5E-07
0.0000001
5E-08
0
0
0.03
0.3
3
Paclitaxel Dose in uM

B.

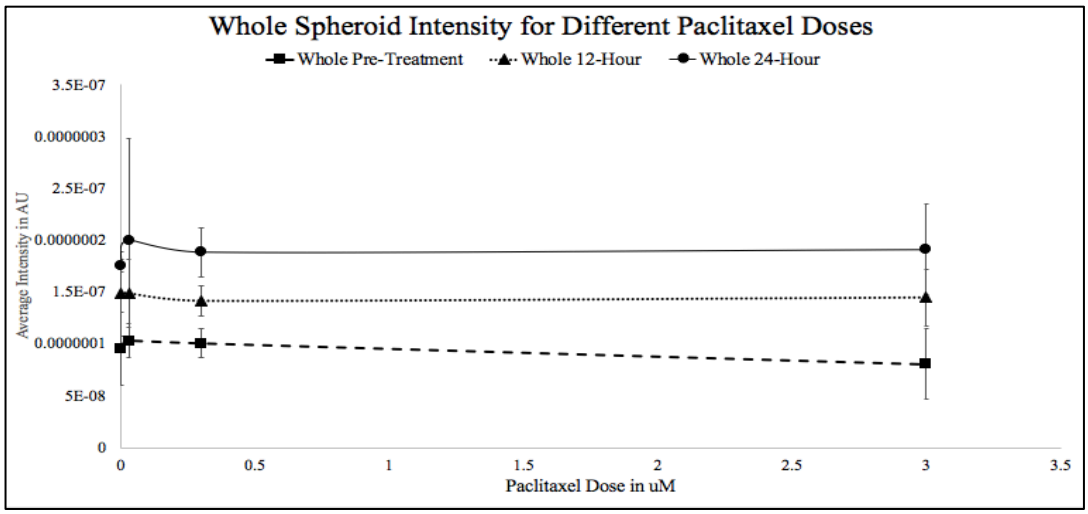

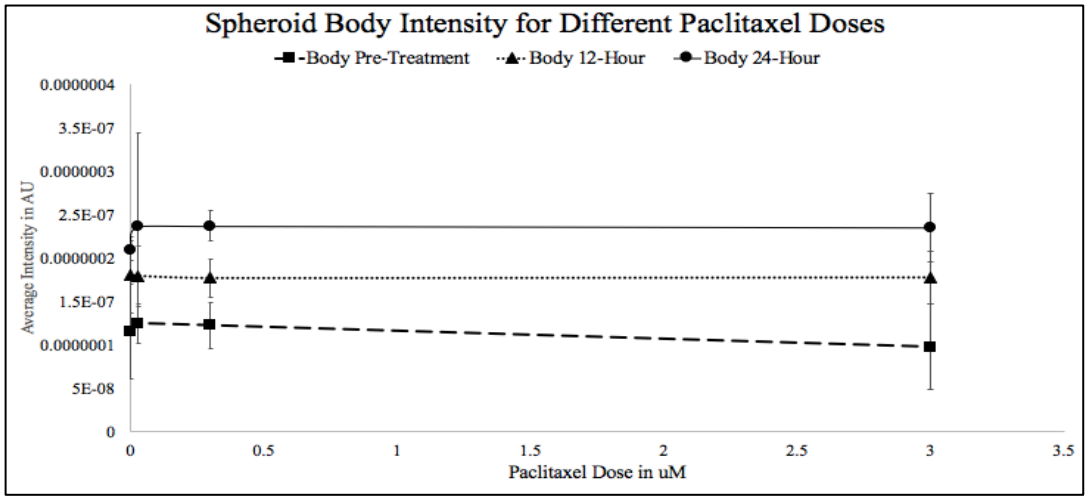

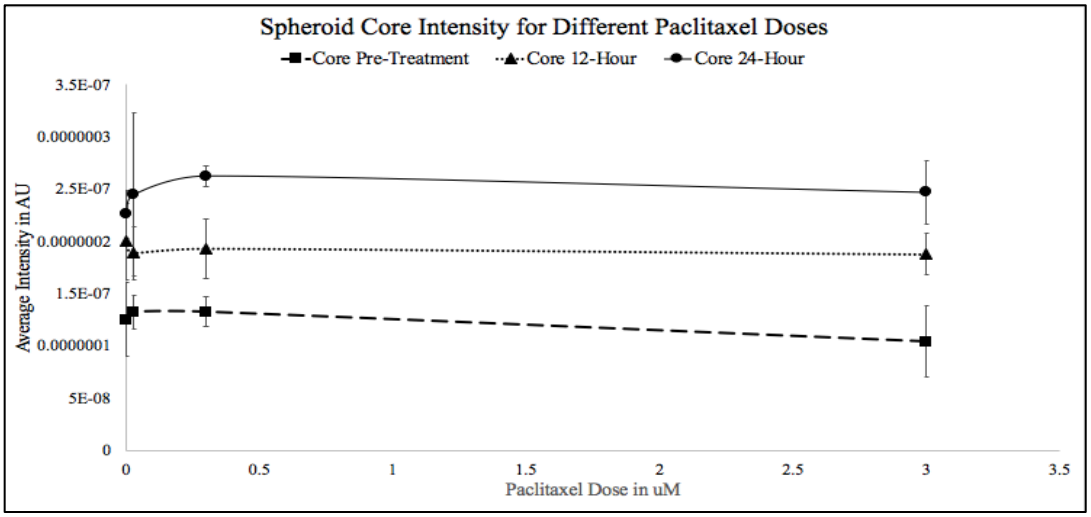

Figure 31. MCF7 spheroid (whole, body and core) intensity plots **A**. by treatment groups; **B**. by doses in line graph form. None of the values were statistically significant when compared with treatment groups. Within treatment groups, single asterisks signify p-value<0.05 and double asterisks signify p-value<0.01.

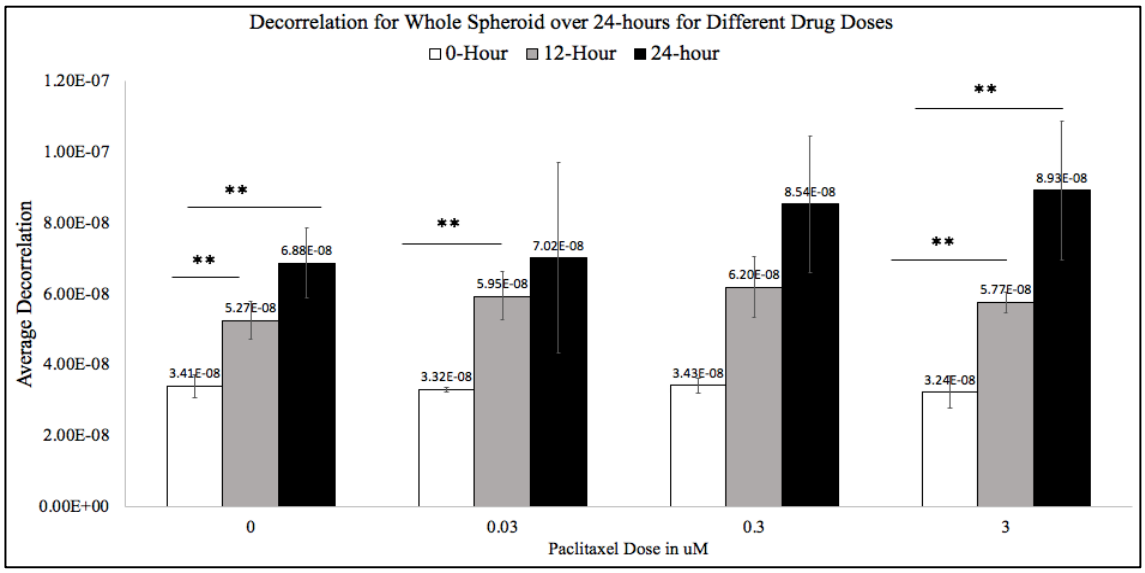
Decorrelation for Whole Spheroid over 24-hours for Different Drug Doses
0-Hour
12-Hour
24-hour
Average Decorrelation
1.20E-07
1.00E-07
8.00E-08
6.00E-08
4.00E-08
2.00E-08
0.00E+00
3.41E-08
5.27E-08
6.88E-08
3.32E-08
5.95E-08
7.02E-08
3.43E-08
6.20E-08
8.54E-08
3.24E-08
5.77E-08
8.93E-08
**
**
**
**
**
0
0.03
0.3
3
Paclitaxel Dose in uM

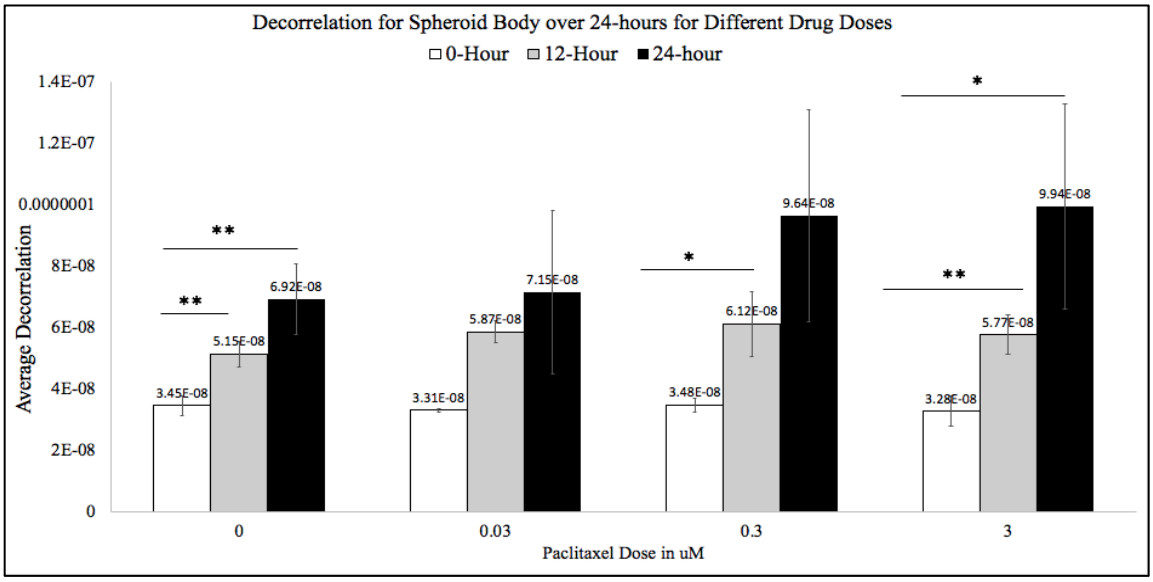
Decorrelation for Spheroid Body over 24-hours for Different Drug Doses
0-Hour
12-Hour
24-hour
Average Decorrelation
1.4E-07
1.2E-07
0.0000001
8E-08
6E-08
4E-08
2E-08
0
3.45E-08
5.15E-08
6.92E-08
3.31E-08
5.87E-08
7.15E-08
3.48E-08
6.12E-08
9.64E-08
3.28E-08
5.77E-08
9.94E-08
**
**
*
**
*
0
0.03
0.3
3
Paclitaxel Dose in uM

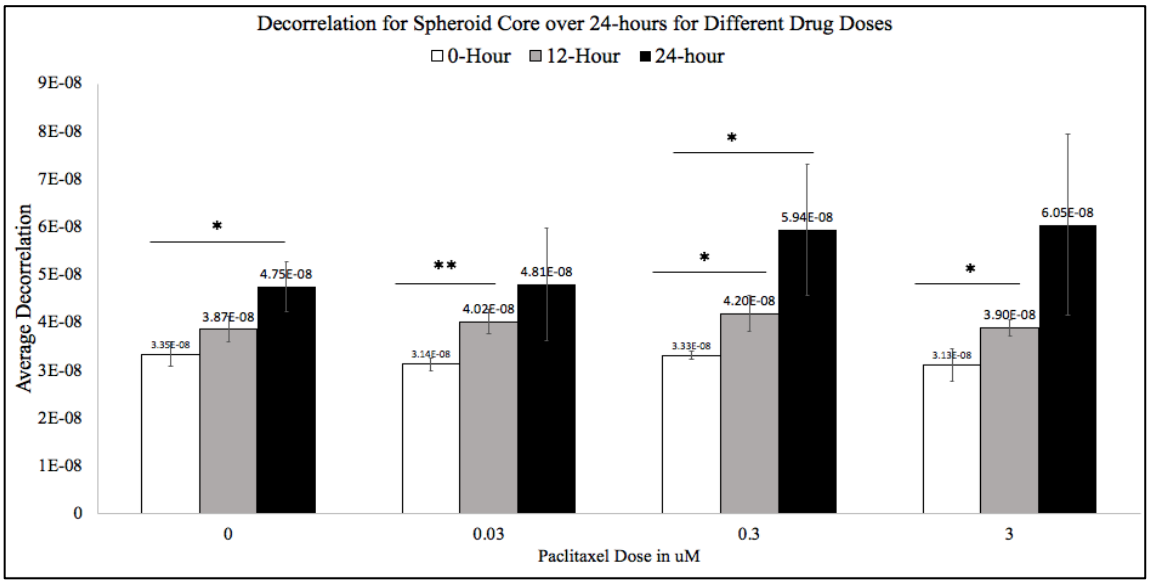
Decorrelation for Spheroid Core over 24-hours for Different Drug Doses
0-Hour
12-Hour
24-hour
Average Decorrelation
9E-08
8E-08
7E-08
6E-08
5E-08
4E-08
3E-08
2E-08
1E-08
0
3.35E-08
3.87E-08
4.75E-08
3.14E-08
4.02E-08
4.81E-08
3.33E-08
4.20E-08
5.94E-08
3.13E-08
3.90E-08
6.05E-08
*
**
*
*
*
0
0.03
0.3
3
Paclitaxel Dose in uM

Figure 32. Decorrelation graphs for all three rounds of experiments averaged and plotted for different drug doses and exposure times. Single asterisks correspond to p-value< 0.05 and double asterisks correspond to p-vale< 0.01.

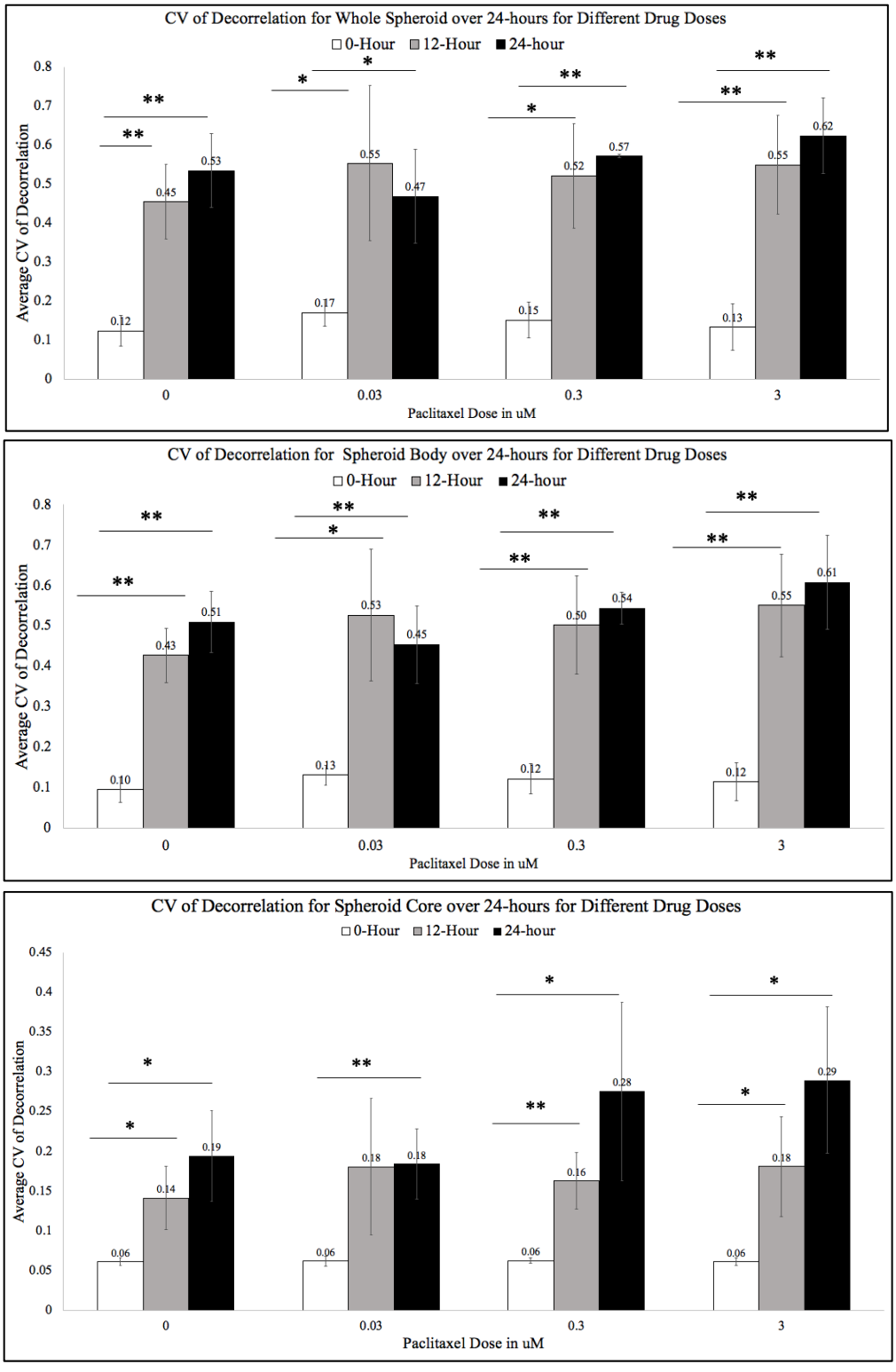

Figure 33. Coefficient of Variation (CV) of Decorrelation for all three rounds of experiments averaged and plotted for different drug doses and exposure times. Single asterisks correspond to p-value< 0.05 and double asterisks correspond to p-vale< 0.01.

As a metric, we looked at both raw decorrelation value (figure 32), the coefficient of variation (CV) (figure 33). CV of decorrelation is independent of intensity, in theory, hence, should provide data with less variability than intensity. Decorrelation allows signal autocorrelation reduction and has been known to provide a measure for intracellular motility, based on previous experiments performed in the Lee lab. Decorrelation depends on the sample intensity, and therefore normalization is required. We noticed that the decorrelation values remained consistently high for the 24-hour time point for whole, body and core regions of the spheroid, but showed no significant differences when all the treatment groups were compared with each other (figure 32). For CV of decorrelation for the whole, body and core regions of the spheroids, we were able to identify the same trend. While the results from the decorrelation analysis is promising, it is interesting to find that the decorrelation at the spheroid cores have been consistently high for all the regions at all the time points. Based on the results from the Live/Dead assay, we found the core of the spheroid housed most of the live cells. Therefore, decorrelation *may* indicate the number of viable cells within a spheroid. Previous studies with *ex vivo* retinal cells in the Lee lab showed that the decorrelation values went down as the pH of a solution became acidic. For this experiment, the pH of the solution became basic, when tested with pH paper (Hydrion, NY) at 12-hours and 24-hours time points. Based on solution pH, the decorrelation values stayed consisted with our previous studies.

However, this representation of decorrelation may not be accurate, since this averages out all the values obtained by the three different regions of interest. Decorrelation provides information about the same location for different time intervals (in this case, 10 ms, 20 ms and 30 ms), and averaging them out may not provide an accurate insight into the intracellular movement. Perhaps filtering this data for each time point for each region and plotting them will help obtain any motion occurring in the spheroid core and throughout the spheroid. In order to conclude whether decorrelation is a direct measure for cellular viability, the samples can be fixed and sectioned for additional histological assessment.

5.2.3 Live/Dead Results

Figure 31 shows a representative panel for the Live/Dead assay fluorescence imaging.

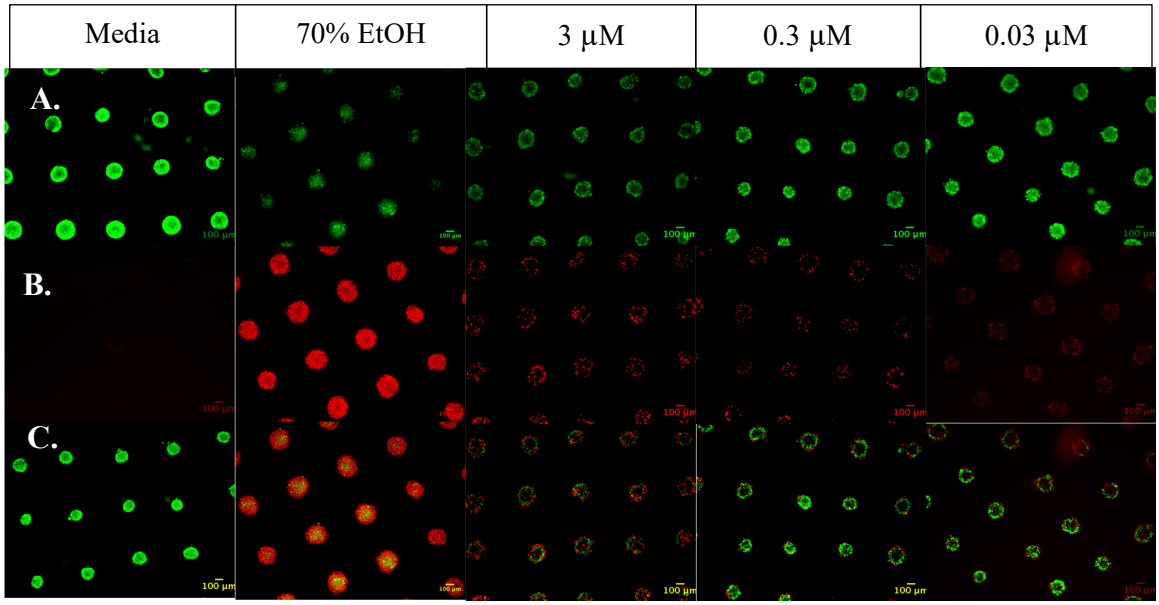

Figure 34. A representative panel of live, dead and combined images of MCF7 spheroids after 24-hours of paclitaxel exposure. Cells were clearly less viable in ethanol control and 3 μM Paclitaxel group (green channel- row A), and the ethanol control had the highest number of dead cells (red channel- row B). Dead cells were observed in paclitaxel treated group, but the visibility feigned as the drug concentration went down (row C shows combined channels). Images were acquired for green, red and brightfield (not shown). Scale bar= 100 μm.

Qualitatively, the live stain was the brightest in the media control and the dead stain was the brightest in the 70% EtOH group, as expected. However, it was interesting to observe that despite a 45-minute exposure to ethanol, the core of the dead control spheroids expressed some green (live) signal. When looking at the Paclitaxel treated groups, the spheroids' edges certainly showed more dead cells than the core of the spheroids. This suggests that the diffusion rate of the two different stains *may* be different. This further validates the need for an additional histology assessment, particularly for the spheroid cores, for understanding cell viability within the spheroids. When we looked at the RID values (averaged and expressed at percentage changes) for a quantitative understanding (Supplemental figure 12), the values for the red channel in all treatment groups was significantly different from the ethanol control (dead control). The RID for green channel, however, showed no significant difference when compared between media control and the drug treated groups. In consequence, the Live/Dead assay did not show any significant cell death in the Paclitaxel-treated groups. Our drug doses might not be high enough, or the manual RID analysis might not be precise. Especially, the data was analyzed without background masking so that the error bars (represented by standard deviation) was so large. The manual process might leave noise in the selected spheroid. Therefore, even though our assay worked (as demonstrated by our assay

controls), the assay could not help us determine the efficacy of the Paclitaxel doses we investigated, in the 3D spheroids.

Chapter 6

6. Conclusion and Future Direction

6.1 Conclusion

So far, we have shown that OCT can be used to image MCF7 spheroids in 3D in a label-free manner over a 24-hour exposure with Paclitaxel, an antiproliferation drug. We identified OCT's accuracy to image spheroids of certain sizes better, over others. With the help of the experiments performed, we also tested two mini incubator prototypes and how they can aid to a longitudinal imaging platform. By means of our image reconstruction, segmentation and analysis codes, we were able to look at various metrics (spheroid volume, area, area to volume ratio, surface roughness, intensity, decorrelation and CV of decorrelation) some of which have been described earlier. We narrowed down our choices of metrics, and we were able to identify whether one metric was superior over another in order to quantify cellular viability for 3D spheroids. We have also performed Live/Dead assay for method validation and to experiment consistency. Even though we would have liked to see significant differences in metrics and identify certain trends, we were unable to notice significant differences in all of our metrics (volume, surface roughness, intensity and decorrelation) when compared between groups, even though the Live/Dead assay showed some death in the Paclitaxel treated

groups. Therefore, it can simply mean that the Paclitaxel doses we have tested were not high enough to kill the MCF7 3D spheroids. Also, literature have shown that Paclitaxel is often monitored for a much longer exposure time than we have tested for. We had the physical limitation of the mini incubator, that could not be ran over 24-hours (or they circuit would short and cause fire), and therefore, we were not able to perform a study with a longer exposure time. This means that Paclitaxel only prevents tumor growth and does not completely kill tumor cells (as some literature also suggests). Therefore, we expected to see significant differences in spheroid growth and not in cellular viability or death. This latter was confirmed by the Live/Dead assay and the OCT intensity and decorrelation metrics. However, the OCT volume metric failed to show significantly lower growth, and instead showed an increase in the spheroid volume. Because the mini incubator did not have a gas-controlled environment, it is difficult to conclude whether the spheroid volume increased due to death by Paclitaxel, or the last of carbon dioxide control. In order to test the effect of lack of gas-control, our pH test of the spheroid media using pH paper (in a sterile environment) before starting the experiment inside the mini incubator (pre-treatment), at 12-hour and at 24-hour showed that the media was highly basic (about 9 or 10, on a scale of 0 to 13), and therefore, the effect of change in media pH cannot be ignored. Also, the analysis code may have assumed the individual cells that resulted from the disaggregation of the spheroids to be one whole spheroid, resulting in larger volumes.

6.2 Further Experiments and Analysis

We are left with several unanswered questions, and thus we have the scope to perform several other experiments and analysis methods as next steps. Even though we could not find a reliable metric for assessing cellular viability in this experiment, we are yet to normalize the decorrelation data to the intensity values. The decorrelation values obtained can be normalized by powers of intensity, autocorrelation-based normalization, hyperbolic tangent fit etc. This is important, since decorrelation depends greatly on the sample intensity, and normalizing the values will lead to decorrelation values independent of the sample depth. This strategy may help find significant results. Another additional step that can be taken on the existing data is performing further statistical analysis. Variance test was not performed in these data sets, and therefore, we can perform a variance test, and if it fails, we can perform Welch's t-test with Bonferroni adjustments to asses significance. We also have the acquired Dynamic Light Scattering (DLS) data from this study, that can be analyzed to provide further information on the newly adjusted parameters for DLS scan before conducting any further experiments.

Based on the data we have obtained so far, this study unveils the potential to use OCT and our analysis system for drug studies in tumor spheroids. Once the aforementioned metrics are investigated, the immediate next step would be to conduct a study where we use higher Paclitaxel concentrations and employ later DIVs if they produce higher growth in control (DIV 5, post spheroid self-assembly). It should be noted though that DIVs later than DIV 3 made spheroids crawl out; thus, a longer DIV with a lower seeding density may be better design for the experiment. Also, in order to

solely assess cellular viability, we can perform combination and sequential drug studies, since Paclitaxel alone may not be able to induce death in tumor cells. Finally, this model can also be expanded for the administration of neoadjuvant chemotherapy in 3D breast cancer spheroids. Together with OCT's ability to perform longitudinal 3D viability assessment and Microtissues^{TM} as a controlled platform for 3D spheroid culture, there is potential for this setup to be used for novel drug safety and efficacy test.

Supplemental Figures

OCT (Lee lab platform)	**Combined DOSI/DCS**	**MCT/DHMCI**	**Raman Spectroscopy**	**Laparoscopic OCT**
Real Time Data (but analysis takes time	No real time data (Data collected and interpreted later)	Real Time useable data	Real time data (but takes a while to analyze)	Real Time Data
Useful for bench setup	Clinically significant and has been used for bench top characterization	Clinically significant (ability to distinguish cell types); Useful for bench setup	Useful for bench setup	Clinically significant
May be high throughput	Not high throughput	High throughput	Not high throughput	Not high throughput
Label free	Label free	Label free	Label free	-
Longitudinal ability	Longitudinal ability	Longitudinal ability (only up to a few hundred minutes)	Longitudinal ability	N/A
Drug study possible	Chemo study performed	Drug study performed	Bee venom study	-
In Vitro 3D tissue	Performed in patient tissue, *in vivo* (characterization *in vivo* too)	*in vitro*- 3D spheroids and *ex vivo* xenografts	*in vitro* 2D	*in vivo, ex vivo*
High statistical power	Variability between instruments, improvement needed	High statistical power	No strong claim of high statistical power	Low statistical power
Intensity	Absorption Coefficient	No relevant metric found	No relevant metric found	No relevant metric found
Decorrelation	No relevant metric found	No relevant metric found	No relevant metric found	No relevant metric found

Up to 12 region specific analysis possible	N/A	Shell and core analysis	N/A	N/A
Non-invasive technique	Invasive	Non-invasive technique	Non-invasive technique	Invasive
Able to image an entire microtissue with a large enough FOV	n= 34 subjects	n= 131 (UMR spheroids); n= 40 (DLD-1 and HT-29 spheroids); n= 32 (PcCa2 spheroids)	n= 10 at a time (2D)	One location at a time
Can potentially test combination, sequential and neoadjuvant therapies	Standard chemo and neoadjuvant hormonal therapy	Antiproliferation drugs have been tested	Bee venom tested (in a relevant study setup)	-
Has been tested for 24-hour longitudinal study	~4 months in patients	120 minutes	12 hr, 24 hr, 48 hr, 72 hr	-

Supplemental Figure 1. Comparison of Different Imaging Systems against Lee Lab's OCT.

Experiment Number	**Number of Microtissue *per Seeding Density***	**Number of Spheroids Analyzed**	**Total Number of Spheroids *per Seeding Density***
Exp. 1	3	n= 16	48
Exp. 2	3	n= 16	48
Exp. 3	3	n= 16	48

Supplemental Figure 2. Sample distribution for each experiment for cell seeding density.

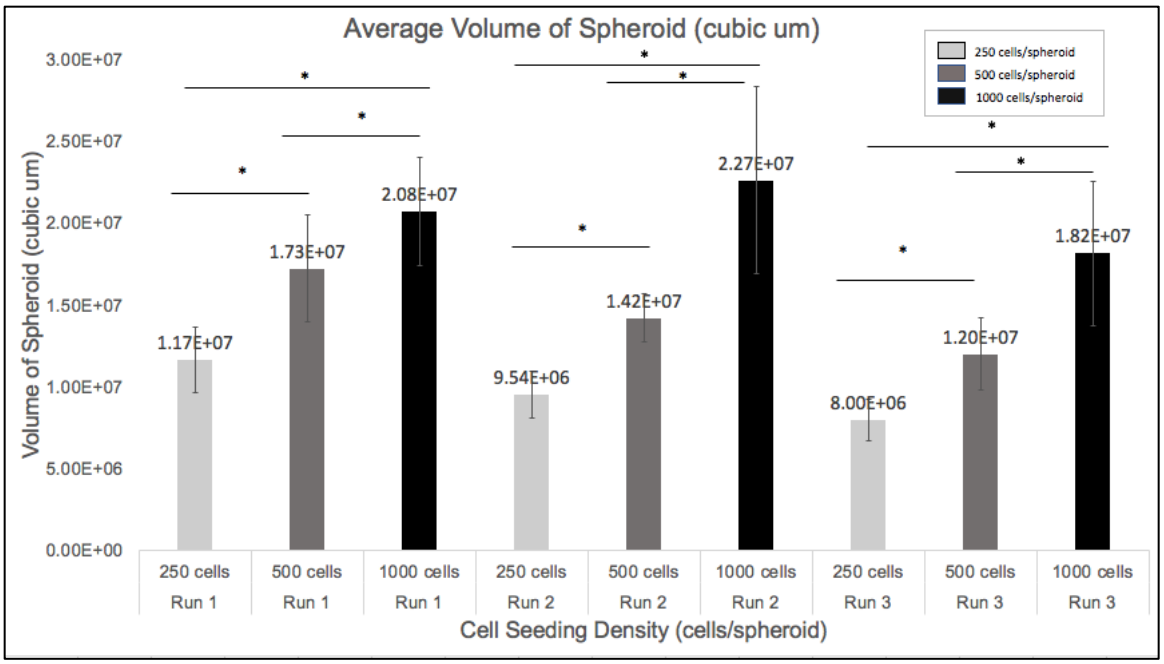

Supplemental Figure 3. Average spheroid volumes (measured in cubic micrometers) for different spheroid seeding densities. Volumes were significantly different for each seeding density. The asterisks indicate p-values< 0.01.

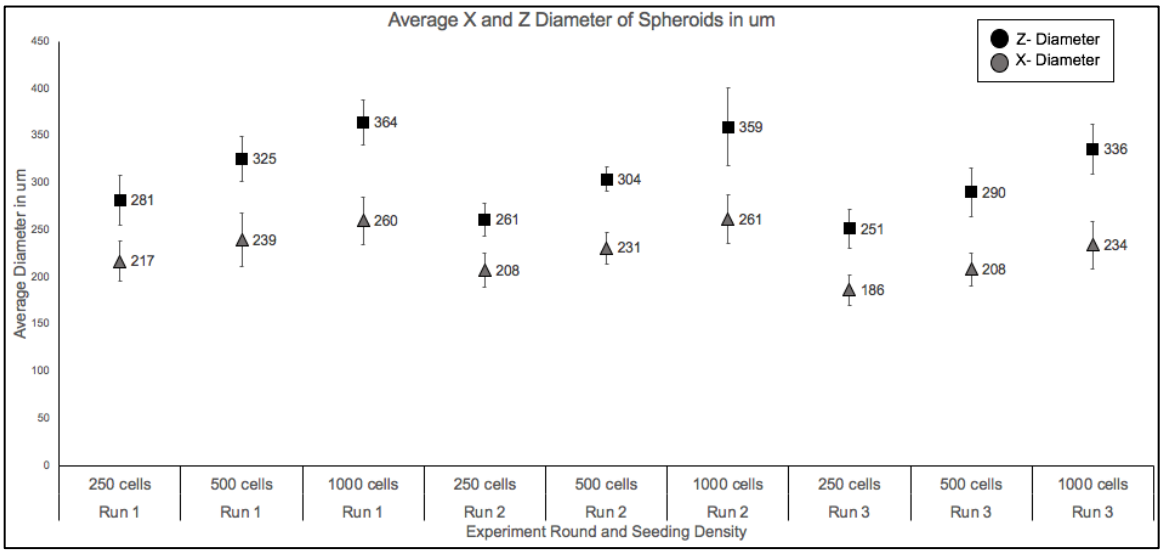

Supplemental Figure 4. Average spheroid diameter for different seeding densities, with a dz value of 3.5 µm.

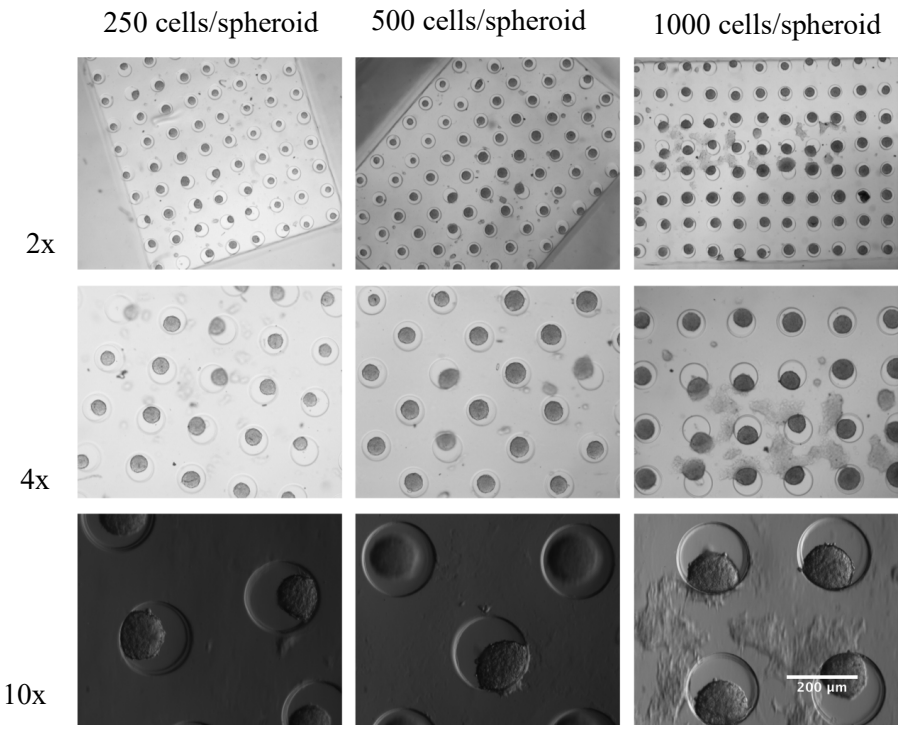

Supplemental Figure 5. Microtissues with MCF7 cells at DIV=2 for different magnifications, showing ‘crawling out' phenomenon in the spheroids.

Tube	Media (µL)	DMSO Stock (µL)	PTX Stock 2 (µL)	Total Volume (µL)
Conc. 1 (3.0 µM)	3500	0	1500	5000
Conc. 2 (0.3 µM)	3500	1350	150	5000
Conc.3 (0.03 µM)	3500	1485	15	5000
Control	3500	1500	0	5000

Supplemental Figure 6. Working solutions of Paclitaxel (from 1 mM stock) for MCF7 treatment. DMSO Stock refers to a 1% DMSO in culture media solution (5000 µL final volume). PTX Stock 2 refers to a 10 µM paclitaxel solution in culture media.

	Run 1			Run 2			Run 3		
Treatment- Replicate	Dyn Range	oseg	ns	Dyn Range	oseg	ns	Dyn Range	oseg	ns
H-1	0.90-0.99	s2	14	0.85-0-99	s1	20	0.75-0.99	c1	16
H2	0.90-0.99	c2	14	0.92-0-99	c2	16	0.75-0.99	c1	16
M-1	0.85-0.99	c2	16	0.95-0.99	c2	16	0.85-0.99	s2	16
M-2	0.85-0.99	s2	14	0.75-0.99	c2	16	0.85-0.99	s2	16
L-1	0.85-0.99	s2	10	0.85-0.99	c2	16	0.92-099	c2	16
L-2	0.85-0.99	s2	10	0.90-0.99	s2	14	0.92-099	c2	16
0-1	0.85-0.99	s2	16	0.85-0.99	c2	16	0.85-0.99	c3 (big cloud)	12
0-2	0.90-0.99	c2	10	0.90-0.99	c2	16	0.85-0.99	c2	12

Supplemental Figure 7. Dynamic range measurements (dyn range), segmentation options (oseg) and number of spheroids (ns) selected for data segmentation for the main study.

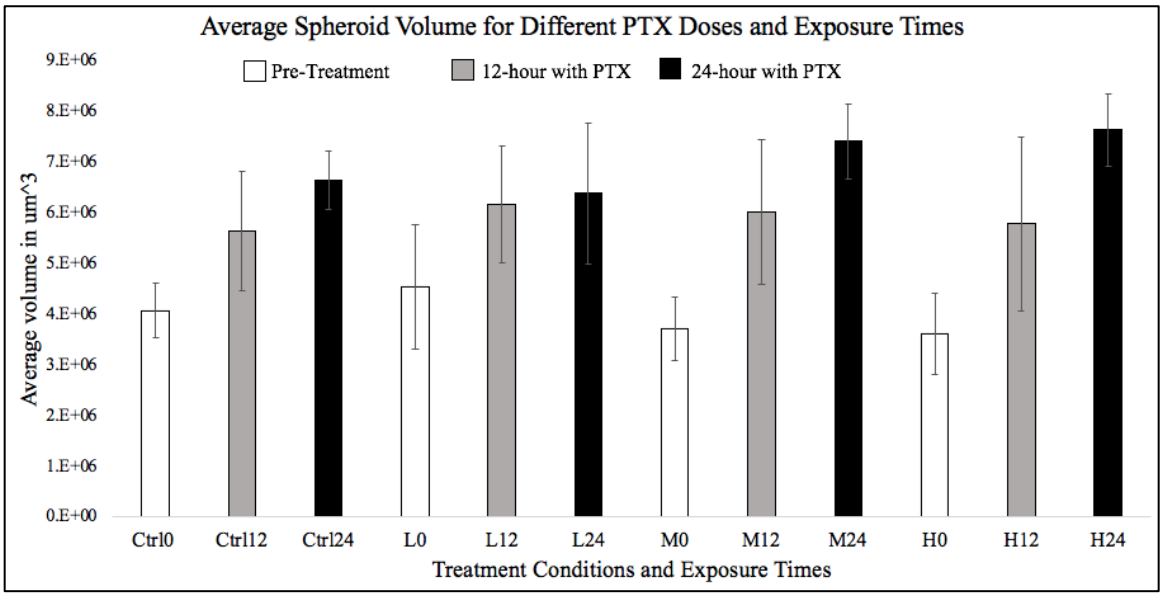

Supplemental Figure 8. Averaged absolute spheroid volumes for different treatment conditions and exposure times.

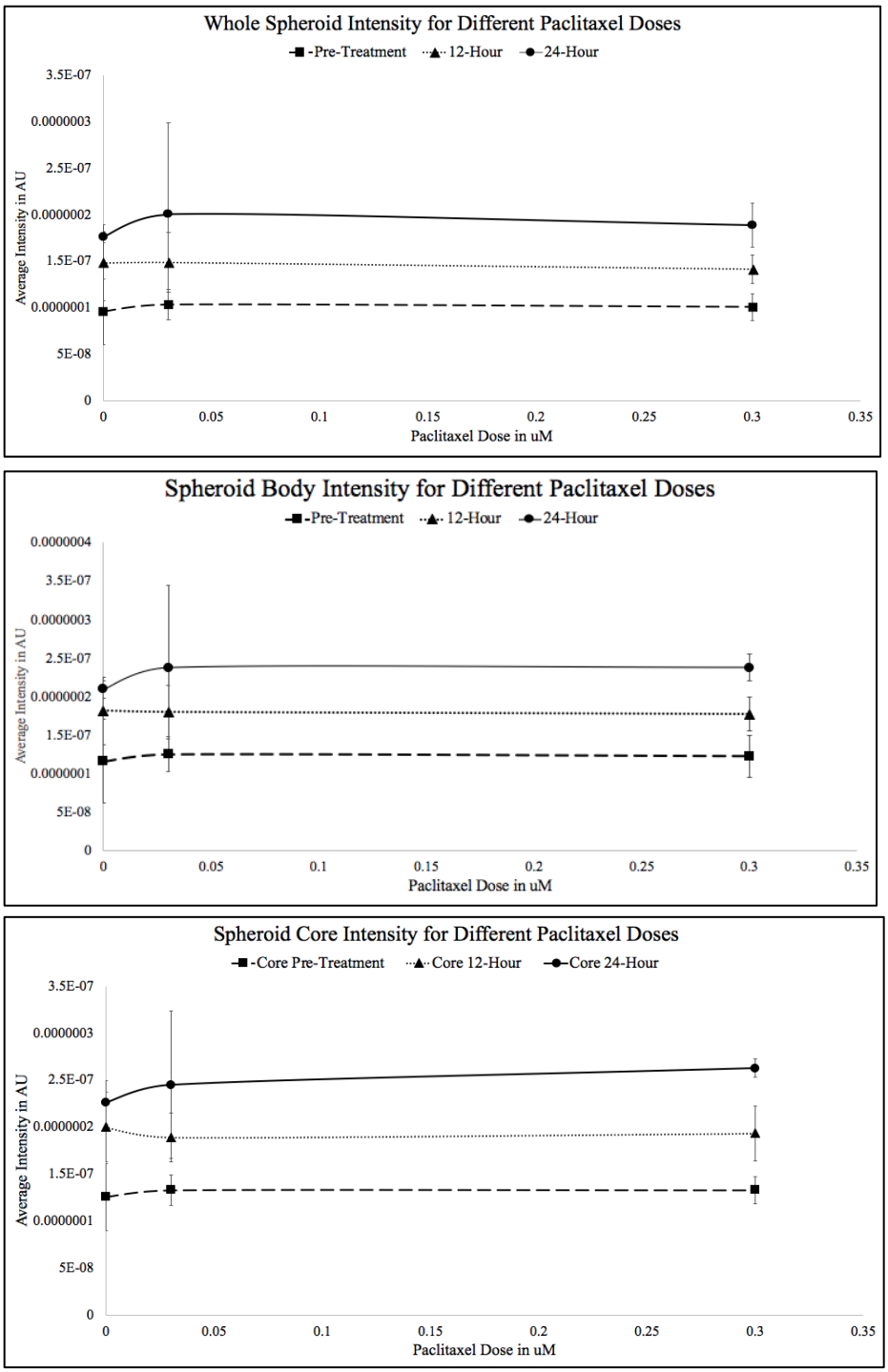

Supplemental Figure 9. Intensity plots showing the change in intensity for 0.03 and 0.3 uM Paclitaxel doses.

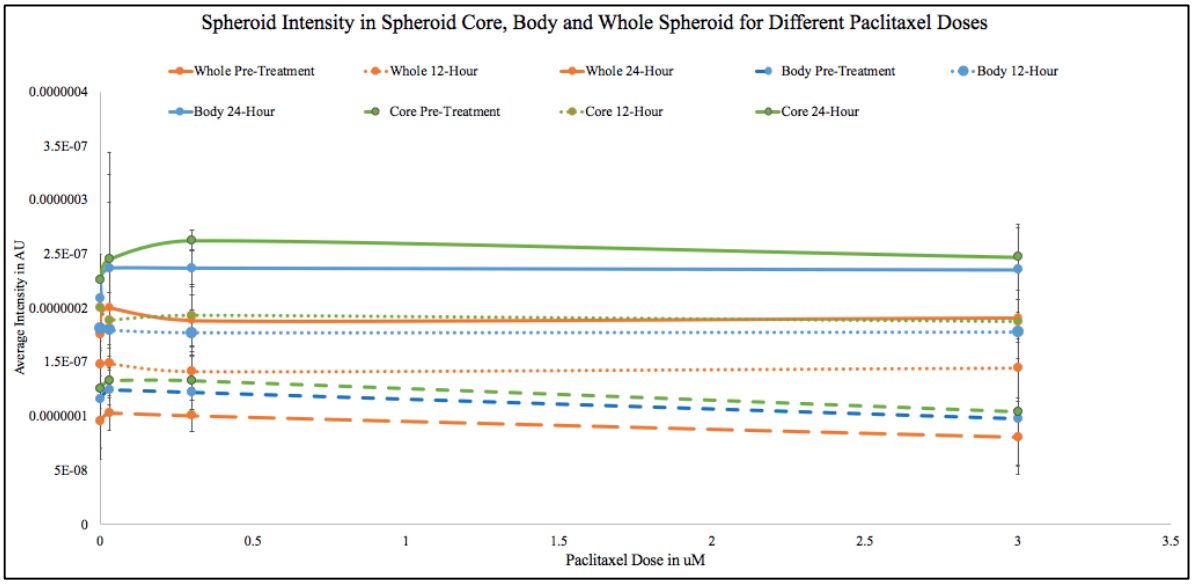

Supplemental Figure 10. The average spheroid intensities (whole, body and core) for different treatment conditions and exposure times all plotted in the same graph.

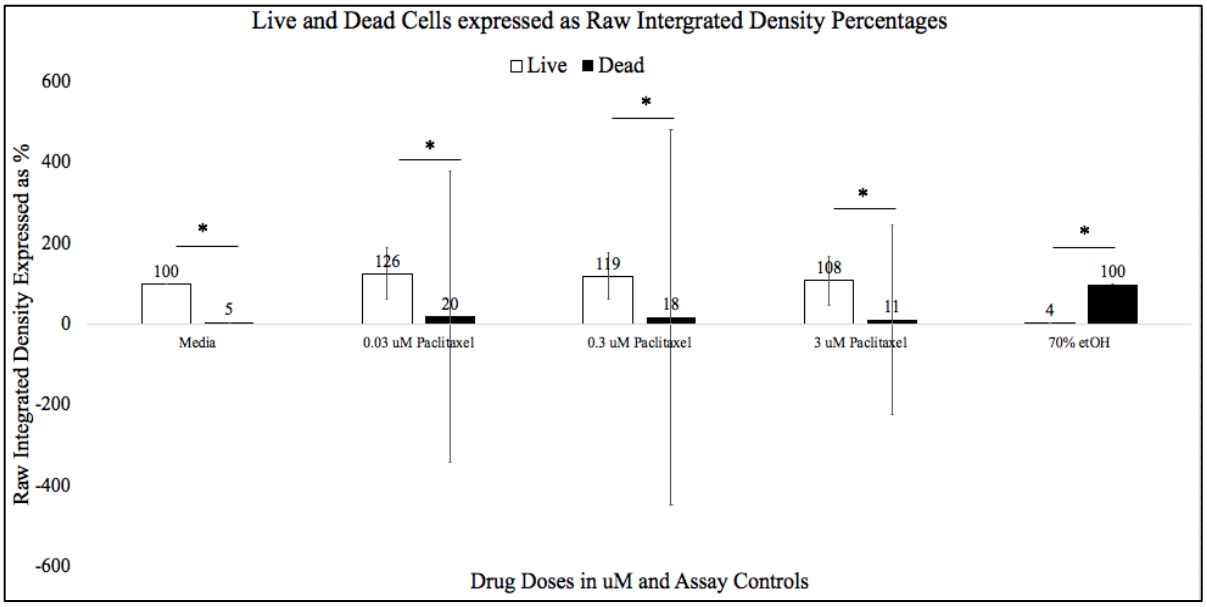

Supplemental Figure 11. Raw Integrated Density percentages for live/dead assay. Other than the indicated significance, the values were significantly different for the red channel (dead stain) for all the groups when compared to the 70% ethanol control group. The green channel (live stain) was not significantly different for any of the drug treatment groups when compared to the media control group. Asterisks indicate p-value<0.05.

Bibliography

[1] “Breast Cancer Facts & Figures.” American Cancer Society, www.cancer.org/research/cancer-facts-statistics/breast-cancer-facts-figures.html.

[2] Comşa, Şerban, and ANCA MARIA CÎMPEAN. and. “The Story of MCF-7 Breast Cancer Cell Line: 40 Years of Experience in Research.” Anticancer Research, International Journal of Cancer Research and Treatment, 1 June 2015, ar.iiarjournals.org/content/35/6/3147.full.

[3] “MCF7 (ATCC® HTB-22™).” MCF7 ATCC® HTB-22™, www.atcc.org/Products/All/HTB-22.aspx.

[4] Levenson, Anait S., and V. Craig Jordan. “MCF-7: The First Hormone-Responsive Breast Cancer Cell Line.” Cancer Research, 1997.

[5] Lippman, Marc E., and Gail Bolan. “Oestrogen-Responsive Human Breast Cancer in Long Term Tissue Culture.” Nature, 1975, doi:10.1038/256592a0.

[6] Reynolds, Daniel S., et al. “Breast Cancer Spheroids Reveal a Differential Cancer Stem Cell Response to Chemotherapeutic Treatment.” Scientific Reports, 2017, doi:10.1038/s41598-017-10863-4.

[7] Edmondson, Rasheena, et al. “Three-Dimensional Cell Culture Systems and Their Applications in Drug Discovery and Cell-Based Biosensors.” Assay and Drug Development Technologies, 2014, doi:10.1089/adt.2014.573.

[8] Cukierman, E., et al. “Taking Cell-Matrix Adhesions to the Third Dimension.” Science, 2001, doi:10.1126/science.1064829.

[9] Pineda, Emma T., et al. “Differentiation Patterns of Embryonic Stem Cells in Two- versus Three-Dimensional Culture.” Cells Tissues Organs, 2013, doi:10.1159/000346166.

[10] Anton, Delphine, et al. “Three-Dimensional Cell Culture: A Breakthrough in Vivo.” International Journal of Molecular Sciences, 2015, doi:10.3390/ijms16035517.

[11] Dingle, Yu Ting L., et al. “Three-Dimensional Neural Spheroid Culture: An In Vitro Model for Cortical Studies.” Tissue Engineering - Part C: Methods, 2015, doi:10.1089/ten.tec.2015.0135.

[12] Frantz, Christian, et al. “The Extracellular Matrix at a Glance.” Journal of Cell Science, 2010, doi:10.1242/jcs.023820.

[13] Baharvand, Hossein, et al. “Differentiation of Human Embryonic Stem Cells into Hepatocytes in 2D and 3D Culture Systems in Vitro.” International Journal of Developmental Biology, 2006, doi:10.1387/ijdb.052072hb.

[14] Dittmar, Roman, et al. “Assessment of Cell Viability in Three-Dimensional Scaffolds Using Cellular Auto-Fluorescence.” Tissue Engineering - Part C: Methods, 2012, doi:10.1089/ten.tec.2011.0334.

[15] Lin, Ruei Zhen, and Hwan You Chang. “Recent Advances in Three-Dimensional Multicellular Spheroid Culture for Biomedical Research.” Biotechnology Journal, 2008, doi:10.1002/biot.200700228.

[16] McGuire, WP, et al. “Taxol: A Unique Antineoplastic Agent with Significant Activity in Advanced Ovarian Epithelial Neoplasms.” International Journal of Gynecology & Obstetrics, 1990, doi:10.1016/0020-7292(90)91032-l.

[17] Reichman, B. S., et al. “Paclitaxel and Recombinant Human Granulocyte Colony-Stimulating Factor as Initial Chemotherapy for Metastatic Breast Cancer.” Journal of Clinical Oncology, 1993, doi:10.1200/JCO.1993.11.10.1943.

[18] Bharadwaj, Rajnish, and Hongtao Yu. “The Spindle Checkpoint, Aneuploidy, and Cancer.” Oncogene, 2004, doi:10.1038/sj.onc.1207374.

[19] Napolitano, Anthony P., et al. “Scaffold-Free Three-Dimensional Cell Culture Utilizing Micromolded Nonadhesive Hydrogels.” BioTechniques, 2007, doi:10.2144/000112591.

[20] Napolitano, Anthony P., et al. “Dynamics of the Self-Assembly of Complex Cellular Aggregates on Micromolded Nonadhesive Hydrogels.” Tissue Engineering, 2007, doi:10.1089/ten.2006.0190.

[21] Monazzam, Azita, et al. “Application of the Multicellular Tumour Spheroid Model to Screen PET Tracers for Analysis of Early Response of Chemotherapy in Breast Cancer.” Breast Cancer Research, 2007, doi:10.1186/bcr1747.

[22] Imamura, Yoshinori, et al. “Comparison of 2D- and 3D-Culture Models as Drug-Testing Platforms in Breast Cancer.” Oncology Reports, 2015, doi:10.3892/or.2015.3767.

[23] Wu, Jia, et al. “Identifying Relations between Imaging Phenotypes and Molecular Subtypes of Breast Cancer: Model Discovery and External Validation.” Journal of Magnetic Resonance Imaging, 2017, doi:10.1002/jmri.25661.

[24] Bhadriraju, Kiran, and Christopher S. Chen. “Engineering Cellular Microenvironments to Improve Cell-Based Drug Testing.” Drug Discovery Today, 2002, doi:10.1016/S1359-6446(02)02273-0.

[25] Fleming, Jodie M., et al. “In Situ Drug Delivery to Breast Cancer-Associated Extracellular Matrix.” ACS Chemical Biology, 2018, doi:10.1021/acschembio.8b00396.

[26] Li, Linfeng, et al. “High-Throughput Imaging: Focusing in on Drug Discovery in 3D.” Methods, 2016, doi:10.1016/j.ymeth.2015.11.013.

[27] Lemmo, Stephanie, et al. “Optimization of Aqueous Biphasic Tumor Spheroid Microtechnology for Anti-Cancer Drug Testing in 3D Culture.” Cellular and Molecular Bioengineering, 2014, doi:10.1007/s12195-014-0349-4.

[28] Hutmacher, Dietmar W., et al. “Can Tissue Engineering Concepts Advance Tumor Biology Research?” Trends in Biotechnology, 2010, doi:10.1016/j.tibtech.2009.12.001.

[29] Mehta, Geeta, et al. “Opportunities and Challenges for Use of Tumor Spheroids as Models to Test Drug Delivery and Efficacy.” Journal of Controlled Release, 2012, doi:10.1016/j.jconrel.2012.04.045.

[30] Zaha, Dana Carmen. “Significance of Immunohistochemistry in Breast Cancer.” World Journal of Clinical Oncology, 2014, doi:10.5306/wjco.v5.i3.382.

[31] Varma, Manoj M., et al. “High-Speed Label-Free Detection by Spinning-Disk Micro-Interferometry.” Biosensors and Bioelectronics, 2004, doi:10.1016/j.bios.2003.12.033.

[32] Harris, Alexandra R., et al. “Assessing Multiparametric Drug Response in Tissue Engineered Tumor Microenvironment Models.” Methods, 2018, doi:10.1016/j.ymeth.2017.12.010.

[33] Jung, Gyeong Bok, et al. “Anti-Cancer Effect of Bee Venom on Human MDA-MB-231 Breast Cancer Cells Using Raman Spectroscopy.” Biomedical Optics Express, 2018, doi:10.1364/boe.9.005703.

[34] An, Ran, et al. “Live Tissue Viability and Chemosensitivity Assays Using Digital Holographic Motility Contrast Imaging.” Applied Optics, 2013, doi:10.1364/AO.52.00A300.

[35] Jeong, Kwan, et al. “Volumetric Motility-Contrast Imaging of Tissue Response to Cytoskeletal Anti-Cancer Drugs.” Optics Express, 2007, doi:10.1364/oe.15.014057.

[36] Dobbs, Jessica, et al. “Confocal Fluorescence Microscopy for Rapid Evaluation of Invasive Tumor Cellularity of Inflammatory Breast Carcinoma Core Needle Biopsies.” Breast Cancer Research and Treatment, 2015, doi:10.1007/s10549-014-3182-5.

[37] Virgone-Carlotta, Angélique, et al. “In-Depth Phenotypic Characterization of Multicellular Tumor Spheroids: Effects of 5-Fluorouracil.” PLoS ONE, 2017, doi:10.1371/journal.pone.0188100.

[38] Vinci, Maria, et al. “Advances in Establishment and Analysis of Three-Dimensional Tumor Spheroid-Based Functional Assays for Target Validation and Drug Evaluation.” BMC Biology, 2012, doi:10.1186/1741-7007-10-29.

[39] Bonafè, Francesca, et al. “Complete Disaggregation of MCF-7-Derived Breast Tumour Spheroids with Very Low Concentrations of α-Mangostin Loaded in CD44 Thioaptamer-Tagged Nanoparticles.” International Journal of Medical Sciences, 2019, doi:10.7150/ijms.28135.

[40] Perche, Federico, and Vladimir P. Torchilin. “Cancer Cell Spheroids as a Model to Evaluate Chemotherapy Protocols.” Cancer Biology and Therapy, 2012, doi:10.4161/cbt.21353.

[41] Friedrich, Juergen, et al. “Spheroid-Based Drug Screen: Considerations and Practical Approach.” Nature Protocols, 2009, doi:10.1038/nprot.2008.226.

[42] Majumder, Biswanath, et al. “Predicting Clinical Response to Anticancer Drugs Using an Ex Vivo Platform That Captures Tumour Heterogeneity.” Nature Communications, 2015, doi:10.1038/ncomms7169.

[43] Hoarau-Véchot, Jessica, et al. “Halfway between 2D and Animal Models: Are 3D Cultures the Ideal Tool to Study Cancer-Microenvironment Interactions?” International Journal of Molecular Sciences, 2018, doi:10.3390/ijms19010181.

[44] Katt, Moriah E., et al. “In Vitro Tumor Models: Advantages, Disadvantages, Variables, and Selecting the Right Platform.” Frontiers in Bioengineering and Biotechnology, 2016, doi:10.3389/fbioe.2016.00012.

[45] Halfter, Kathrin, et al. “Prospective Cohort Study Using the Breast Cancer Spheroid Model as a Predictor for Response to Neoadjuvant Therapy - the SpheroNEO Study.” BMC Cancer, 2015, doi:10.1186/s12885-015-1491-7.

[46] Kessel, Sarah, et al. “Real-Time Viability and Apoptosis Kinetic Detection Method of 3D Multicellular Tumor Spheroids Using the Celigo Image Cytometer.” Cytometry Part A, 2017, doi:10.1002/cyto.a.23143.

[47] Kepp, Oliver, et al. “Cell Death Assays for Drug Discovery.” Nature Reviews Drug Discovery, 2011, doi:10.1038/nrd3373.

[48] Huang, Yongyang, et al. “Optical Coherence Tomography Detects Necrotic Regions and Volumetrically Quantifies Multicellular Tumor Spheroids.” Cancer Research, 2017, doi:10.1158/0008-5472.CAN-17-0821.

[49] Mirzapur, Pegah, et al. “Apoptosis Induction in Human Breast Cancer Cell Lines by Synergic Effect of Raloxifene and Resveratrol through Increasing Proapoptotic Genes.” Life Sciences, 2018, doi:10.1016/j.lfs.2018.04.035.

[50] Lovitt, Carrie J., et al. “Doxorubicin Resistance in Breast Cancer Cells Is Mediated by Extracellular Matrix Proteins.” BMC Cancer, 2018, doi:10.1186/s12885-017-3953-6.

[51] Ye, Jun, et al. “Cellular Uptake Mechanism and Comparative Evaluation of Antineoplastic Effects of Paclitaxel– Cholesterol Lipid Emulsion on Triple-Negative and Non-Triple-Negative Breast Cancer Cell Lines.” International Journal of Nanomedicine, 2016, doi:10.2147/IJN.S113638.

[52] Chhetri, Raghav K., et al. “Longitudinal Study of Mammary Epithelial and Fibroblast Co-Cultures Using Optical Coherence Tomography Reveals Morphological Hallmarks of Pre-Malignancy.” PLoS ONE, 2012, doi:10.1371/journal.pone.0049148.

[53] Oldenburg, Amy L., et al. “Inverse-Power-Law Behavior of Cellular Motility Reveals Stromal–Epithelial Cell Interactions in 3D Co-Culture by OCT Fluctuation Spectroscopy.” Optica, 2015, doi:10.1364/optica.2.000877.

[54] Yu, Xiao, et al. “Quantification of the Effect of Toxicants on the Intracellular Kinetic Energy and Cross-Sectional Area of Mammary Epithelial Organoids by OCT Fluctuation Spectroscopy.” Toxicological Sciences : An Official Journal of the Society of Toxicology, 2018, doi:10.1093/toxsci/kfx245.

[55] Krause, Silva, et al. “The Microenvironment Determines the Breast Cancer Cells’ Phenotype: Organization of MCF7 Cells in 3D Cultures.” BMC Cancer, 2010, doi:10.1186/1471-2407-10-263.

[56] Susienka, Michael J., et al. “Quantifying the Kinetics and Morphological Changes of the Fusion of Spheroid Building Blocks.” Biofabrication, 2016, doi:10.1088/1758-5090/8/4/045003.

[57] Barisam, Maryam, et al. “Prediction of Necrotic Core and Hypoxic Zone of Multicellular Spheroids in a Microbioreactor with a U-Shaped Barrier.” Micromachines, 2018, doi:10.3390/mi9030094.

[58] Eilenberger, Christoph, et al. “Optimized AlamarBlue Assay Protocol for Drug Dose-Response Determination of 3D Tumor Spheroids.” MethodsX, 2018, doi:10.1016/j.mex.2018.07.011.

[59] Millard, Marie, et al. “Drug Delivery to Solid Tumors: The Predictive Value of the Multicellular Tumor Spheroid Model for Nanomedicine Screening.” International Journal of Nanomedicine, 2017, doi:10.2147/IJN.S146927.

[60] Su, Zhenyi, et al. “Apoptosis, Autophagy, Necroptosis, and Cancer Metastasis.” Molecular Cancer, 2015, doi:10.1186/s12943-015-0321-5.

[61] Harris, Adrian L. “Hypoxia - A Key Regulatory Factor in Tumour Growth.” Nature Reviews Cancer, 2002, doi:10.1038/nrc704.

[62] Kessel, Sarah, et al. “Real-Time Viability and Apoptosis Kinetic Detection Method of 3D Multicellular Tumor Spheroids Using the Celigo Image Cytometer.” Cytometry Part A, 2017, doi:10.1002/cyto.a.23143.

[63] Gantenbein-Ritter, Benjamin, et al. “Accuracy of Three Techniques to Determine Cell Viability in 3D Tissues or Scaffolds.” *Tissue Engineering - Part C: Methods*, 2008, doi:10.1089/ten.tec.2008.0313.